Monthly Notices
of the
ROYAL ASTRONOMICAL SOCIETY

MNRAS **477,** 4792–4809 (2018)
Advance Access publication 2018 April 14

doi:10.1093/mnras/sty937

Astrochemical evolution along star formation: overview of the IRAM Large Program ASAI

Bertrand Lefloch,[1,2] R. Bachiller,[3] C. Ceccarelli,[1] J. Cernicharo,[4] C. Codella,[5] A. Fuente,[3] C. Kahane,[1] A. López-Sepulcre,[1,6] M. Tafalla,[3] C. Vastel,[7] E. Caux,[7] M. González-García,[3,4] E. Bianchi,[5,8] A. Gómez-Ruiz,[5,9] J. Holdship,[10] E. Mendoza,[2] J. Ospina-Zamudio,[1] L. Podio,[5] D. Quénard,[10] E. Roueff,[11] N. Sakai,[12] S. Viti,[10] S. Yamamoto,[13] K. Yoshida,[13] C. Favre,[5] T. Monfredini,[14] H. M. Quitián-Lara,[14] N. Marcelino,[4] H. M. Boechat-Roberty[14] and S. Cabrit[15]

[1] *CNRS, IPAG, Univ. Grenoble Alpes, F-38000 Grenoble, France*
[2] *IAG, Universidade de São Paulo, Cidade Universitária, 05508-090 São Paulo, SP, Brazil*
[3] *IGN Observatorio Astronómico Nacional, Apartado 1143, E-28800 Alcalá de Henares, Spain*
[4] *Group of Molecular Astrophysics, ICMM, CSIC, C/Sor Juana Inés de La Cruz N3, E-28049 Madrid, Spain*
[5] *INAF, Osservatorio Astrofisico di Arcetri, Largo Enrico Fermi 5, I-50125 Firenze, Italy*
[6] *IRAM, 300 rue de la Piscine, F-38406 Saint-Martin d' Hères, France*
[7] *Université de Toulouse, UPS-OMP, IRAP, 31028 Toulouse, France*
[8] *Dipartimento di Fisica e Astronomia, Università degli Studi di Firenze, Via G. Sansone 1, I-50019 Sesto Fiorentino, Italy*
[9] *CONACYT-Instituto Nacional de Astrofísica, Optica y Electrónica, Luis E. Erro 1, 72840 Tonantzintla, Puebla, México*
[10] *Department of Physics and Astronomy, UCL, Gower St, London WC1E 6BT, UK*
[11] *Sorbonne Université, Observatoire de Paris, Université PSL, CNRS, LERMA, F-92190 Meudon, France*
[12] *The Institute of Physical and Chemical Research (RIKEN), Wako, Saitama 351-0198, Japan*
[13] *Department of Physics, University of Tokyo, Bunkyo-ku, Tokyo 113-0033, Japan*
[14] *Observatorio do Valongo, UFRJ, 20080-090 Rio de Janeiro, Brazil*
[15] *Sorbonne Université, Observatoire de Paris, Université PSL, CNRS, LERMA, F-75014 Paris, France*

Accepted 2018 March 22. Received 2018 March 9; in original form 2017 November 4

ABSTRACT

Evidence is mounting that the small bodies of our Solar system, such as comets and asteroids, have at least partially inherited their chemical composition from the first phases of the Solar system formation. It then appears that the molecular complexity of these small bodies is most likely related to the earliest stages of star formation. It is therefore important to characterize and to understand how the chemical evolution changes with solar-type protostellar evolution. We present here the Large Program 'Astrochemical Surveys At IRAM' (ASAI). Its goal is to carry out unbiased millimetre line surveys between 80 and 272 GHz of a sample of 10 template sources, which fully cover the first stages of the formation process of solar-type stars, from pre-stellar cores to the late protostellar phase. In this paper, we present an overview of the surveys and results obtained from the analysis of the 3 mm band observations. The number of detected main isotopic species barely varies with the evolutionary stage and is found to be very similar to that of massive star-forming regions. The molecular content in O- and C-bearing species allows us to define two chemical classes of envelopes, whose composition is dominated by either (a) a rich content in O-rich complex organic molecules, associated with hot corino sources, or (b) a rich content in hydrocarbons, typical of warm carbon-chain chemistry sources. Overall, a high chemical richness is found to be present already in the initial phases of solar-type star formation.

Key words: astrochemistry – stars: formation – ISM: abundances – ISM: jets and outflows – ISM: molecules.

* E-mail: bertrand.lefloch@univ-grenoble-alpes.fr

1 INTRODUCTION

Understanding 'our chemical origins', i.e. the evolution of matter during the long process that brought it from pre-stellar cores, to protostars, protoplanetary discs, and eventually to the bodies of the Solar system, is one of the most active topics in contemporary astrophysics (Caselli & Ceccarelli 2012).

Once the gravitational collapse is underway, the forming star is at the centre of a thick envelope, from where it accretes matter. Class 0 sources represent the first stages of the collapse (e.g. André, Ward-Thompson & Barsony 1993). The innermost envelope regions, with a size of a few 100 au, known as *hot corinos*, are heated by the radiation emitted by the central object and the ices are sublimated. The molecules forming the ices are thus liberated and injected into the gas phase, where they may undergo further reactions. They share similarities with hot cores but are not just scaled-down versions of them (Bottinelli et al. 2007). Hot corinos are similar in size and composition to the nebula precursor of the Solar system (see e.g. Jaber et al. 2014), so that their study can be considered as archaeological study of our Solar system.

Only a handful of hot corinos have been identified so far (IRAS 16293−2422: Cazaux et al. 2003; IRAS2 and IRAS4B: Bottinelli et al. 2007; IRAS4A: Bottinelli et al. 2004a; Taquet et al. 2015; HH 212: Codella et al. 2016; L483: Oya et al. 2017; B335: Imai et al. 2016). Their nature and their molecular composition remain unclear: IRAS 16293 is the only hot corino investigated in detail until now (Caux et al. 2011; Jørgensen et al. 2012, 2016; Jaber et al. 2014), and may not be representative of the whole Class 0. As a matter of fact, Sakai et al. (2008) have discovered a different type of chemically distinct Class 0 protostars, the so-called warm carbon-chain chemistry (WCCC) sources, that are C-chain enriched, but unlike hot corinos poor in complex organic molecules (COMs). The actual composition of all these protostars, their similarities and differences, and their origin (that could be related to the infall dynamics) remain yet to be established. The protostellar phase plays a major role in building up the molecular complexity, as highlighted by the recent detection of pre-biotic molecules, like e.g. glycolaldehyde (Jørgensen et al. 2012) and formamide (Kahane et al. 2013) around the solar-type protostar IRAS 16293−2422.

Evidence is mounting that the small bodies of our Solar system, such as comets and asteroids, have at least partially inherited their chemical composition from the first phases of the Solar system formation. For example, the molecular abundances in Comet Hale–Bopp were found to be similar to those in the protostellar outflow L1157 (Bockelée-Morvan et al. 2000), and the HDO/H_2O ratio measured in the ice of comets is, within a factor of 2, equal to the ocean value (Mumma & Charnley 2011; Ceccarelli et al. 2014). Moreover, the large deuteration of amino acids in meteorites suggests that at least a fraction of them were formed during the first phases of the Solar system (Pizzarello & Huang 2005).

Thanks to the recent spectacular progress of radio astronomical and far-infrared observatories, detailed observations of systems at different evolutionary stages have become possible, and these can shed light on the most decisive chemical processes determining the evolution. However, despite a wealth of fragmentary studies in the literature, the characterization and understanding of the chemical evolution along solar-type protostellar evolution are far from being achieved.

Systematic spectral line surveys constitute the most powerful diagnostic tool to carry out a comprehensive study of the chemical evolution of star-forming regions. In general terms, as transitions with different upper energy levels and Einstein coefficients are excited at different temperatures and densities, line surveys permit to efficiently probe different regions along the line of sight (see e.g. Tercero et al. 2010; Caux et al. 2011). Star-forming regions are particularly complex because of their strong spatial chemical differentiation and because different lines from the same species are excited under different conditions (temperature, density, velocity field, etc.), with sometimes complex kinematics, where infall and outflow motions are simultaneously present.

Unbiased spectral surveys of low-mass, solar-type objects have been carried out so far only towards TMC1 and Barnard 1 (Marcelino et al. 2009; Cernicharo et al. 2012), IRAS 16293 (Blake et al. 1994; Caux et al. 2011; Jørgensen et al. 2016), IRAS4 (Blake et al. 1995), L1527 at 3 mm only (Takano et al. 2011), and R CrA IRS7B at 0.8 mm (Watanabe et al. 2012). Now, the new capabilities of the Institute for Radio Astronomy in the Millimeter Range (IRAM) 30 m telescope have made it possible to take a major step forward in the investigation of molecular complexity along with star formation, by observing with unprecedented sensitivity the emission of molecular rotational transitions in the millimetre domain, from 80 to 272 GHz, in a greatly reduced amount of time.

With all this in mind, we have undertaken a Large Program Astrochemical Studies At IRAM (ASAI)[1] to characterize and to understand the chemical evolution along solar-type protostellar evolution. To do so, we have used the IRAM 30 m telescope to carry out unbiased millimetre line surveys of a sample of template sources, which cover the full formation process of solar-type stars, from pre-stellar cores to protoplanetary discs. The objective of this paper is to describe the general characteristics of the survey: observational strategy, methods of the data analysis, and features of the target, together with some overall and first results (some of them already published in dedicated papers) illustrating the richness of the obtained data.

In this presentation paper of the project, we have focused on the molecular content of the 3 mm band (80–116 GHz). It is the only band that was observed towards all the template sources, with the exception of AB Aur. The systematic approach of our Large Program allows us to draw some first conclusions on the molecular richness of sources as a function of their evolutionary status. The detailed ASAI data analysis including the bands at 2 and 1.3 mm is still under way. Further results on the different sources, transversal studies, and a full analysis of the survey will be presented in forthcoming papers.

2 THE SOURCE SAMPLE

We have selected a sample of 10 template sources illustrating the different chemical stages a solar-type star undergoes during its formation process, presented in Table1.

TMC1 is a quiescent dense ridge in Heiles Cloud 2 at $d \simeq 140$ pc (Cernicharo & Guélin 1987) in the Taurus molecular cloud complex. It is characterized by a very rich molecular spectrum and strong chemical differences along the ridge, and is considered as an ideal source to study the chemistry of dark clouds (e.g. Pratap et al. 1997; Liszt & Ziurys 2012). The position observed here, 'the cyanopolyyne peak', is particularly rich in carbon chains, including radicals and cyanopolyynes, and it was previously surveyed in the 3-mm band with the IRAM 30 m radio telescope (see Marcelino et al. 2007, 2009; Cernicharo et al. 2012). Among the molecules detected in these previous surveys with the 30 m IRAM telescope

[1] http://www.oan.es/asai/

Table 1. Source and observational characteristics. The first four columns refer to the source name, coordinates, distance, and luminosity. The following columns report the observed spectral windows and the range of rms noise achieved in a 1 km s^{-1} channel for each spectral window. The rms values (in T_A^*) are measured in the range 86–87 and 113–114 GHz at 3 mm, 132–133 and 169–170 GHz at 2 mm, and 220–221 and 260–261 GHz at 1 mm.

Sources	Coordinates (J2000)	d (pc)	Lum. ($L_\odot$)	3 mm (mK)	2 mm (mK)	1.3 mm (mK)	δv (kHz)	Comment
TMC1	$04^h41^m41\overset{s}{.}90$ $+25\,°41'27\overset{''}{.}1$	140	–	–	4.2–4.2	–	48.8, 195.3	Early pre-stellar core
L1544	$05^h04^m17\overset{s}{.}21$ $+25\,°10'42\overset{''}{.}8$	140	–	2.1–7.0	–	–	48.8	Evolved pre-stellar core
B1b	$03^h33^m20\overset{s}{.}80$ $+31\,°07'34\overset{''}{.}0$	230	0.77	2.5–10.6[a]	4.4–8.0	4.2–4.6	195.3	First hydrostatic core
L1527	$04^h39^m53\overset{s}{.}89$ $+26\,°03'11\overset{''}{.}0$	140	2.75	2.1–6.7[a]	4.2–7.1	4.6–4.1	195.3	Class 0/I WCCC
IRAS4A	$03^h29^m10\overset{s}{.}42$ $+31\,°13'32\overset{''}{.}2$	260	9.1	2.5–3.4	5.0–6.1	4.6–3.9	195.3	Class 0 hot corino
L1157-mm	$20^h39^m06\overset{s}{.}30$ $+68\,°02'15\overset{''}{.}8$	250	3	3.0–4.7	5.0–6.5	3.8–3.5	195.3	Class 0
SVS 13A	$03^h29^m03\overset{s}{.}73$ $+31\,°16'03\overset{''}{.}8$	260	34	2.0–4.8	4.2–5.1	4.6–4.3	195.3	Class I
AB Aur[b]	$04^h55^m45\overset{s}{.}84$ $+30\,°33'33\overset{''}{.}0$	145	–	4.6–4.3	4.8–3.9	2.1–4.3	195.3	Protoplanetary disc
L1157-B1	$20^h39^m10\overset{s}{.}20$ $+68\,°01'10\overset{''}{.}5$	250	–	1.1–2.9	4.6–7.2	2.1–4.2	195.3	Outflow shock spot
L1448-R2	$03^h25^m40\overset{s}{.}14$ $+30\,°43'31\overset{''}{.}0$	235	–	2.8–4.9	6.0–9.7	2.9–4.9	195.3	Outflow shock spot

[a]3 mm coverage until 112 GHzonly. rms is measured in the range 110–111 GHz. [b]Uncomplete coverage for AB Aur: 85–96, 134–145, 200–208, 216.4–228, 232.6–240, 248.3–256.2, and 264.2–272 GHz.

it is worth noting the completely unexpected saturated propene molecule CH_3CHCH_2 (Marcelino et al. 2007).

L1544 is a starless core in the Taurus molecular cloud complex ($d \simeq 140$ pc; Cernicharo & Guélin 1987) on the verge of the gravitational collapse (Caselli et al. 2012, and references within). It is considered the prototype of pre-stellar cores. Its central high density (2×10^6 cm^{-3}) and very low temperature (∼7 K) generate a chemistry typical of the interiors of dark clouds in which CO is depleted and the deuterium fractionation is high, although differentiated chemical processes can take place in the external layers (Caselli et al. 1999; Vastel et al. 2006, 2014, 2015b, 2016).

Barnard 1 is a dense core in the Perseus molecular complex (Bachiller & Cernicharo 1984, 1986) at $d \simeq 230$ pc (Hirano & Liu 2014). It contains several active star-forming sites of which the position studied here, B1b, is one of the most interesting because of its rich molecular spectrum (Bachiller, Menten & del Rio Alvarez 1990a; Cernicharo et al. 2012; Daniel et al. 2013). B1b was previously surveyed in the 3 mm band with the IRAM 30 m radio telescope by Marcelino et al. (2009) and Cernicharo et al. (2012). It consists of two objects B1-bN and B1-bS, separated by approximately 18 arcsec (Pezzuto et al. 2012; Gerin et al. 2015), which have been proposed as candidates for the first hydrostatic core (FHSC) stage based on the properties of their spectral energy distribution and their outflows (Gerin et al. 2015; Fuente et al. 2017). Both sources have a low luminosity of 0.28 and 0.49 $L_\odot$, respectively (Pezzuto et al. 2012). The targeted position lies approximately halfway between B1-bN and B1-bS (see Table 1). We have reported in Table 1 the total luminosity of the system (0.77 $L_\odot$). Several molecular species have been detected, some of them of high importance for astrochemistry, such as NH_3D^+ (Cernicharo et al. 2013), CH_3O (Cernicharo et al. 2012), and HCNO, the high-energy isomer of isocyanic acid (Marcelino et al. 2009). The source exhibits a large deuteration, as evidenced by the detection of multiply deuterated species such as D_2CS (Marcelino et al. 2005), ND_2H (Roueff et al. 2005), and ND_3 (Lis et al. 2002). Also, a very high abundance in sulfur compounds was reported by Marcelino et al. (2005) and Fuente et al. (2016).

L1527 is a dark cloud in the Taurus molecular complex ($d \simeq$ 140 pc) containing IRAS 04368+2557, a protostar with a luminosity of 2.75 $L_\odot$ (Tobin et al. 2013). Recently, Robitaille et al. (2007) and Tobin et al. (2013) proposed that L1527 probably lies at an intermediate stage Class 0/I, more evolved than previously thought. The position observed here is the nominal position of the protostar from which emerges a highly collimated molecular outflow (Hogerheijde et al. 1998). The complex kinematical structure of the region around the protostar has been recently investigated with Atacama Large Millimeter/submillimeter Array (ALMA) by Oya et al. (2015) and Sakai et al. (2017). This source is considered as a prototypical WCCC source (Sakai et al. 2008, 2010; Sakai & Yamamoto 2013).

NGC 1333-IRAS4A is a binary Class 0 source located in the Perseus molecular complex at $d \simeq 260$ pc (Schlafly et al. 2014). The two components, IRAS4A1 and IRAS4A2, have a separation of about 1.8 arcsec (∼420 au) and a total luminosity of 9.1 $L_\odot$ (Karska et al. 2013). The IRAS4A system is associated with a spectacular large-scale (a few arcminutes) bipolar molecular outflow (e.g. Blake et al. 1995; Choi 2001, 2005; Yildiz et al. 2012; Santangelo et al. 2014). High angular resolution observations by Santangelo et al. (2015) have disentangled two distinct molecular jets powered by each of the two components. IRAS4A was the subject of a spectral line survey between 200 and 400 GHz with the Caltech Submm Observatory (CSO) and the James Clerk Maxwell Telescope (JCMT) by Blake et al. (1995). The weakness of the lines made it impossible to obtain a complete coverage of the spectral windows. Thanks to more recent, sensitive observations with the IRAM 30 m telescope, IRAS4A was identified as a hot corino protostar, the second one after IRAS 16293−2422 (Bottinelli et al. 2007). Santangelo et al. (2015) and López-Sepulcre et al. (2017) confirmed that only source IRAS4A2 is a hot corino protostar, in agreement with the previous detections of dimethyl ether (CH_3OCH_3), ethyl cyanide (C_2H_5CN), and water ($H_2^{18}O$) by Persson, Jørgensen & van Dishoeck (2012); also, de Simone et al. (2017) reported the detection of glycolaldehyde (CH_2OHCHO). Interestingly, no COM emission is detected towards IRAS4A1.

L1157-mm (IRAS 20386+6751) is the Class 0 source driving the powerful L1157 molecular outflow (Bachiller, Martin-Pintado & Fuente 1993; Gueth, Guilloteau & Bachiller 1996; Bachiller et al. 2001; Tafalla et al. 2015) in a quite isolated dark cloud in Cepheus at $d \simeq 250$ pc (Looney, Tobin & Kwon 2007). The protostar of ∼3 $L_\odot$ is surrounded by a circumstellar disc and a protostellar envelope embedded in filamentary cloud (Gueth, Bachiller & Tafalla 2003; Looney et al. 2007).

SVS13A is part of the multiple system NGC 1333-SVS13 ($d \simeq$ 260 pc; Schlafly et al. 2014), where 3 mm sources, called A, B, and C, have been identified by interferometric observations (Bachiller et al. 1998; Looney et al. 2007). The angular distance between

A and B is 15 arcsec, while C is 20 arcsec away from A. The luminosity of SVS13A has been estimated to be 34 $L_\odot$ (Tobin et al. 2016). SVS13A itself is a close (70au) binary (VLA4A, VLA4B) in the radio cm (Tobin et al. 2016). Although SVS13A is still deeply embedded in a large-scale (∼6000 au; e.g. Lefloch et al. 1998a) envelope, its extended (>0.07 pc) outflow, associated with the HH7-11 chain (e.g. Lefloch et al. 1998b, and references therein), and its low L_{submm}/L_{bol} ratio (∼0.8 per cent) lead to the classification as a Class I source (e.g. Chen, Launhardt & Henning 2009, and references therein).

AB Aur is one of the best-studied Herbig Ae stars that host a prototypical Herbig Ae disc. Located at $d \simeq 145$ pc in Taurus, the star has a spectral type A0-A1, a mass ∼2.4 $M_\odot$, and a $T_{eff} \simeq 9500$ K (van den Ancker, de Winter & Tjin A Djie 1998). The disc around AB Aur shows a complex structure: it exhibits an asymmetric dust ring at R= 70–140 au from the star (Piétu, Guilloteau & Dutrey 2005; Tang et al. 2012), outer spiral arm features traced by the CO and its isotopologues emission, and inner spiral arms connecting the dusty ring with the star that have been recently imaged by Tang et al. (2017). The chemical structure of the disc has been studied at high resolution in selected molecular lines by Schreyer et al. (2008), Fuente et al. (2010), Guilloteau et al. (2013), and Pacheco-Vásquez et al. (2015, 2016).

L1157-B1 is a bright hotspot in the southern blueshifted lobe of the powerful L1157 outflow ($d \simeq 250$ pc; Looney et al. 2007). This outflow is considered the archetype of the so-called chemically active outflows (Bachiller & Pérez-Gutiérrez 1997; Bachiller et al. 2001; Burkhardt et al. 2016). The richness and intensity of the molecular spectrum from L1157-B1 has made this position a testbed for shock-chemistry models and a favoured target for molecular surveys (e.g. Gusdorf et al. 2008; Codella et al. 2010, 2015; Lefloch et al. 2010, 2012; Yamaguchi et al. 2012; Busquet et al. 2014; Gómez-Ruiz et al. 2015; Holdship et al. 2016). In particular, the emission of the shock region in the 3 mm band was observed recently in an unbiased manner with the 45 m telescope of the Nobeyama Radio Observatory (NRO) by Yamaguchi et al. (2012) and Sugimura et al. (2011).

L1448-R2 is a bright spot in the southern redshifted lobe of the bipolar molecular outflow L1448 (Bachiller et al. 1990b) that is emanating from a ∼11 $L_\odot$ Class 0 protostar in the Perseus molecular complex at $d \simeq 235$ pc. High angular resolution observations in SiO lines (Dutrey, Guilloteau & Bachiller 1997) were found in agreement with a structure of incomplete and fragmented bow shocks caused by discrete episodes of ejection from the central star ('molecular bullets'). Strong H_2O and high-J CO line emission were detected towards this and other L1448 bright spots by Nisini et al. (2000, 2013), Santangelo et al. (2012), and Gómez-Ruiz et al. (2013) indicating the presence of very dense (∼10^6 cm^{-3}) molecular gas at temperatures in excess of 500 K.

As shown in this short presentation of the different sources of the sample, these objects have all been the subject of previous molecular gas studies at millimetre wavelengths. Maps of the molecular emission and the velocity field obtained with both millimetre single-dish telescopes and interferometers are available for several molecular species and were used to model the origin of their emission.

3 OBSERVATIONS

Spectral line surveys of the full source sample were carried out with the IRAM 30 m telescope over six semesters from 2012 September to 2015 March, using the broad-band Eight MIxer Receiver (EMIR) receivers E090, E150, and E230, connected to the Fast Fourier Transform Spectrometers (FFTS) either in the low (50 kHz) or high (200 kHz) spectral resolution mode. The observations were carried out in Wobbler Switching Mode, with a throw of 3 arcmin, in order to ensure a flat baseline across the spectral bandwidth observed. The instrumental set-up was decided according to the sources.

(i) *TMC1*: full coverage of the 3 mm band with a 50 kHz spectral resolution was obtained previously by another team (see e.g. Marcelino et al. 2007, 2009) and will be published elsewhere (Cernicharo, in preparation) Only the 2 mm band was observed. The lower frequency range 130–150 GHz was observed at 50 kHz spectral resolution, and the high-frequency band 150–170 GHz was observed with the FFTS in its 200 kHz resolution mode.

(ii) *L1544*: only the band 72–115GHz was observed, using the FFTS in its 50 kHz resolution mode.

(iii) *Protostars and outflow shocks* (B1b, L1527, IRAS4A, L1157-mm, SVS13A, L1157-B1, and L1448-R2): the 3 mm (80–116 GHz) and 2 mm (126–170 GHz) bands were observed simultaneously. The 1.3 mm (200–272 GHz) band was covered observing both lower sideband (LSB) and upper sideband (USB) simultaneously using the FFTS in its 200 kHz resolution mode. Complementary observations of the band 72–80 GHz were obtained in 2016 January for L1527, IRAS4A, L1157-mm, SVS13A, and L1157-B1.

(iv) *AB Aur*: the spectral line density is so low that it was decided to perform very deep integrations of a few spectral bands of 4–8 GHz only, instead of covering the full spectral windows. Observations and results are presented in Pacheco-Vásquez et al. (2015).

Whereas E090 and E230 are 2SB receivers, most of the observations in the 2 mm band were carried out with the 'old' E150 receiver, providing an effective instantaneous bandwidth of 4 GHz in double polarization H and V. A 2SB receiver at 2 mm was installed at the IRAM 30 m telescope in 2014 Summer, allowing full coverage of the band 130–150 GHz for TMC1. Observations were carried out with very good to excellent, stable weather conditions. The half-power beamwidth (HPBW) of the IRAM 30 m telescope is described with a good accuracy by the HPBW(arcsec) = 2460/frequency(GHz). The typical beamwidth of the ASAI observations lies therefore in the range 21–34, 14–19, and 9–12 arcsec at 3, 2, and 1.3 mm, respectively.

Pointing was carefully checked every hour on bright nearby continuum sources: NGC 7538 (L1157-B1 and L1157-mm), 0316+413 and 0333+321 (B1, IRAS4A, and SVS13A), and 0439+360 (TMC1, L1527, and L1448-R2). Pointing corrections were always less than 3 arcsec. Focus corrections were done at the beginning of each observing session. They were repeated every 6 h, or when relevant temperature changes occurred (e.g. after sunrise or sunset). Focus corrections were always below 1 mm.

Image band rejection of the EMIR receivers usually ranges between −10 and −20 dB, depending on the frequency (see e.g. IRAM report by Maier 2014). The sensitivity of the ASAI observations is so high that line contamination from the image band cannot be ignored. In order to permit easy identification of lines from the image band in the spectrum, it was decided to regularly shift the frequency of the local oscillator (LO) by a fixed amount of 50 MHz. Spurious features in the spectral bands were identified and subsequently corrected for, in close collaboration with the IRAM receiver engineers group (see e.g. IRAM report by Kramer et al. 2014 for more details).

Contamination by the nearby reference position was observed towards IRAS4A, SVS13A, L1448-R2, and L1527 for bright molecular lines like CO, ^{13}CO, HCO^+, and HCN, for instance. The corresponding spectral settings were re-observed in position switching

mode with a 'clean' reference position, checked to be free of emission.

Data reduction was performed using the GILDAS/CLASS software.[2] A simple flat baseline was first subtracted to each spectra and spectra with very high noise were discarded. From comparing every scan with their (50 MHz LO) frequency shifted counterpart, spurious signals from the image band could be identified and removed. The resulting scans were then averaged in order to produce the final spectral bands. In the 3 mm bands, the final rms lies in the range 2–5mK per interval of 1 km s^{-1}, depending on the frequency.

For each source, the observed position, the nominal spectral resolution of the observations, and the rms achieved in the covered spectral bands are summarized in Table 1. The official ASAI repositories are at Observatorio Astronomico Nacional (OAN)[3] and IRAM.[4] The ASAI data base provides fully reduced, calibrated spectra.

The achieved rms of the ASAI data is similar to that of the TIMASS survey of IRAS 16293−2422 (Caux et al. 2011). As mentioned in Section2, two sources of our sample have been previously surveyed in the same spectral range: IRAS4A and L1157-B1. In the first case, the JCMT–CSO survey by Blake et al. (1995) yielded a typical rms of about 100 mK. In the second case, the NRO 45 m survey by Yamaguchi et al. (2012) and Sugimura et al. (2011) yielded an rms of 4–10 mK per channel of 1 MHz. By comparison, the rms of the ASAI is ≈1–3 mK per element of resolution of 0.3 MHz.

4 OVERALL RESULTS

The spectra of the different targets exhibit very significant differences, reflecting the evolutionary stage and the physical conditions of the different sources. This is illustrated in Figs 1–3, which display the emission in the spectral bands 91.1–94.5 GHz (Fig. 1), 144.1–147.2 GHz (Fig. 2), and 250.2–252.9 GHz (Fig.3). An example is provided by the emission of the cyanomethyl radical (CH_2CN) lines at 100600MHz (see Fig.A1). Bright CH_2CN emission is detected mainly towards the early sources (pre-stellar cores TMC1 and L1544, first hydrostatic core candidate B1b) and the WCCC protostar L1527. There is a striking anticorrelation with the emission of methyl cyanide CH_3CN, a chemically related species, whose emission is extremely bright towards the more evolved and luminous sources (IRAS4A, SVS13A, and L1157-B1) and faint towards the early sources. Only the low-excitation transitions of CH_3CN are detected towards the CH_2CN-rich sources, and their lines are much narrower than those of CH_3CN. A detailed modelling of the CH_2CN and CH_3CN emission in the ASAI sample is currently going on (Vastel, in preparation).

Comparison of the COM emission in the range 90 100–90 258 MHz provides another interesting example of the chemical differentiation that can be observed between the sources of the sample (Fig.A2). This band was chosen as it contains several rotational transitions of ethanol (C_2H_5OH), methyl formate (CH_3OCHO), and formic acid (HCOOH). The signatures of COMs are absent of the pre-stellar core (PSC; TMC1 and L1544) and the WCCC sources (L1527 and L1157-mm), and SVS13A (Class I). On the contrary, they are detected with a very good signal-to-noise ratio (SNR) towards B1b, IRAS4A, and L1157-B1. Linewidths increase markedly from FHSC to Class 0 and to the shock region L1157-B1. It is remarkable that such bright COM emission is detected towards the outflow shock region L1157-B1, whereas no emission is detected in the envelope of the protostar L1157-mm and the initial gas and dust chemical conditions are very similar. The diversity of spectral signatures was also found to reflect the diversity of excitation and chemical conditions among the sample sources. This is well illustrated by the analysis of the CO line profiles detected towards the shock region L1157-B1 by Lefloch et al. (2012).

We used the CASSIS[5] software (Vastel et al. 2015a) for the line identification, using the Cologne Database for Molecular Spectroscopy (CDMS;[6] Müller et al. 2005) and Jet Propulsion Laboratory (JPL)[7] data bases (Pickett et al. 1998). We considered all the lines detected with an intensity higher than 3σ.

We examine here how much the molecular content differs between sources, based on the molecular line identification in the 3 mm band.

4.1 Molecular content

We have classified the identified molecular species in 'elemental families': carbon, nitrogen, oxygen, sulfur, silicon, and phosphorus bearing.

(i) The carbon family contains only hydrocarbons C_xH_y.
(ii) The oxygen family contains only molecules of the type $C_xH_yO_z$.
(iii) The nitrogen family contains only molecules of the type $C_xH_yO_zN_t$.
(iv) The sulfur family contains any sulfur-bearing molecules, of the type $C_xH_yO_zN_tS_u$.
(v) The silicon (phosphorus) family contains any Si-bearing (P-bearing) species.

These definitions are of course incomplete from a chemical point of view, when considering the molecular reaction network associated with each elemental family. A simple molecule like SO is obviously involved in both the sulfur and oxygen chemical networks. The above definitions are introduced for the sake of the analysis that follows hereafter, as they permit identification of evolutionary trends in the gas chemical composition.

Some molecular species were identified from their rare isotopomers (D, ^{13}C): they are indicated with a dagger (†) in Table2. In a few cases, species missed by ASAI in the 3 mm band were known to be present thanks to their signature in the 2 and 1.3 mm bands, like SO^+ or H_2CO. These few species are marked with an asterisk (∗) in Table 2. In the case of water, we have mentioned the detection of the main isotopologue by *Herschel* when the rare isotopomers HDO and $H_2^{18}O$ were not detected by ASAI. This is the case for L1544 (Caselli et al. 2012), L1527 (Karska et al. 2013), and L1448-R2 (Nisini et al. 2013). We also note that H_2COH^+ was marginally detected towards B1b by Fuente et al. (2016), thanks to higher sensitivity observations. These cases are rare enough that they should significantly affect neither the statistics nor our conclusions. Of course, the difference of main beam filling factors between extended sources (pre-stellar cores and shocks) and compact, strongly diluted hot corino sources, influence to some extent the conclusions of this analysis and this study will be extended to the analysis of the 2 and 1.3 mm, for which such a bias effect is less pronounced. On the other hand, the spatial distribution of the

[2] http://www.iram.fr/IRAMFR/GILDAS/
[3] http://www.oan.es/asai
[4] http://www.iram.fr/ILPA/LP007/
[5] http://cassis.irap.omp.eu
[6] http://www.astro.uni-koeln.de
[7] http://spec.jpl.nasa.gov

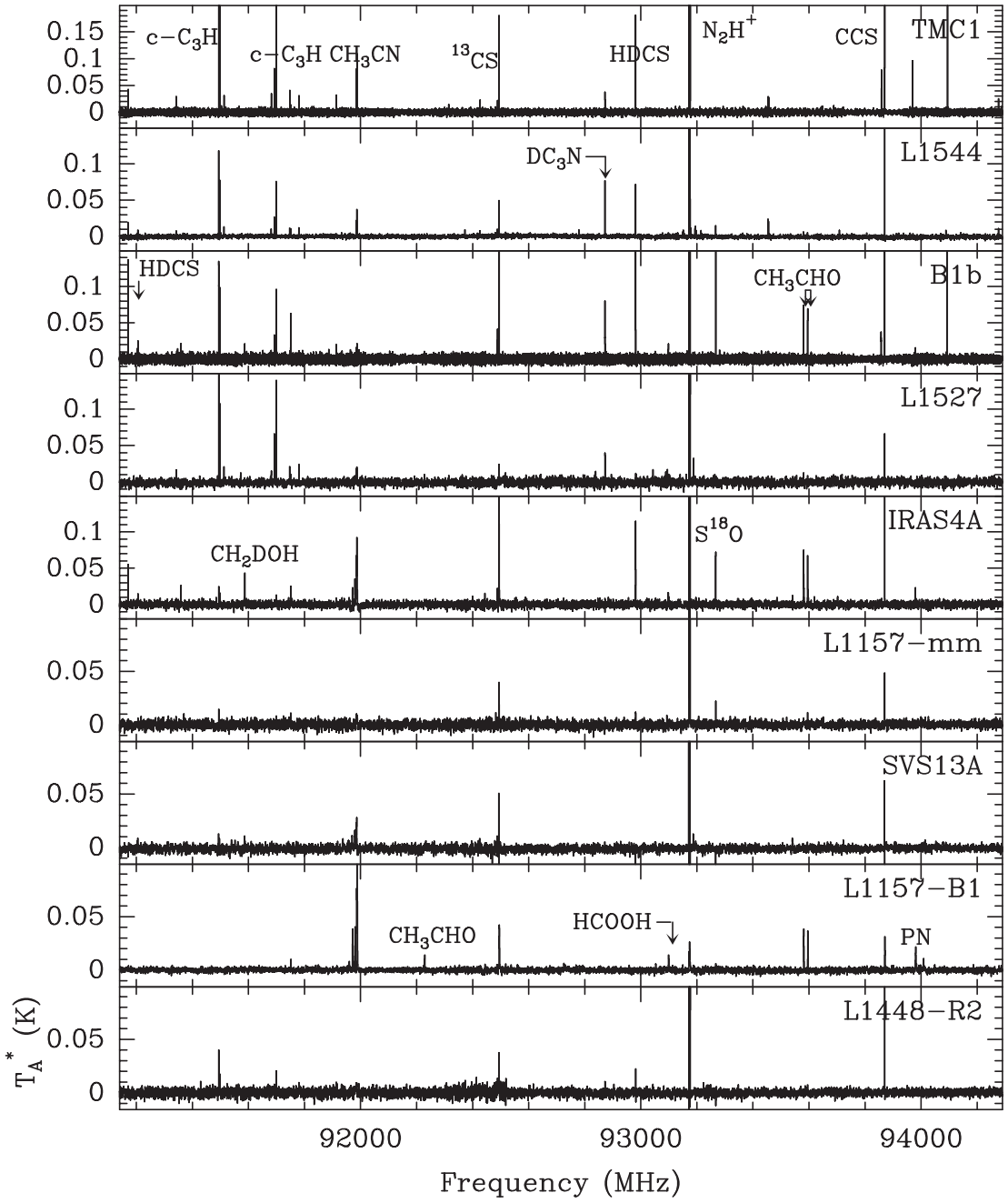

Figure 1. Molecular line emission detected with ASAI in the spectral bands: 91100–94300MHz. The spectral resolution is 350 kHzfor all sources, except for TMC1 (100 kHz). The TMC1 data were taken from Marcelino et al. (2009).

molecular emission also conveys some important information on the source chemistry.

The new generation of interferometers such as ALMA and Northern Extended Millimeter Array (NOEMA) reveals the presence at a much smaller angular scale of additional molecular species, which are missed by sensitive single-dish surveys such as ASAI. So far, only IRAS 16293−2422 has been investigated in an unbiased manner in the course of the Protostellar Interferometric Line Survey (PILS; Jørgensen et al. 2016). Thanks to ALMA, spectral signatures of glycolaldehyde CH_3OHCHO (Jørgensen et al. 2012), acetic acid CH_3COOH, ethylene glycol $(CH_2OH)_2$ (Jørgensen et al. 2016), and ethanol C_2H_5OH (Lykke et al. 2017) have been detected towards IRAS 16293−2422. Some of the of the ASAI sources have been studied at high angular resolution (and high sensitivity with ALMA and NOEMA; see e.g. López-Sepulcre et al. 2017), but there is no coherent data set in terms of frequency range, sensitivity, and angular resolution for the whole ASAI source sample.

We first made an inventory of the number of molecular species, counting separately the main isotopologues and the rare isotopologues detected. The detection of the latter crucially depends on the sensitivity of the survey and the gas column density. Hence, the number of detected isotopologues and molecular lines is a better indicator of the excitation conditions, whereas the number of main isotopologues rather traces the molecular complexity of the source.

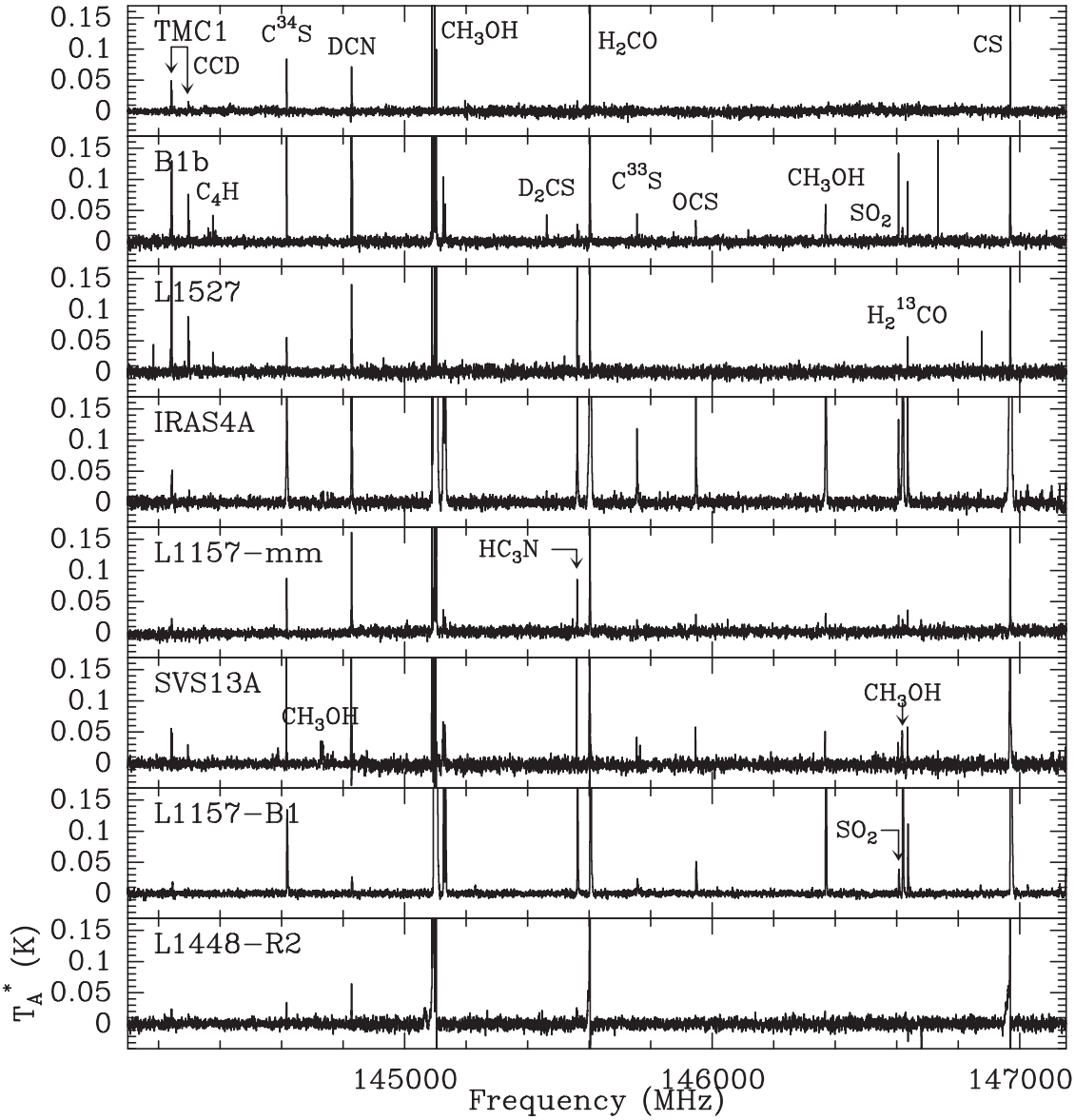

Figure 2. Molecular line emission detected with ASAI in the spectral bands 144100–147200MHz. The spectral resolution is 500 kHz for all the sources.

The results are summarized in Tables 2 and 3, with the exception of TMC1, which was not observed at 3 mm. For the sake of comparison, we have included IRAS 16293−2422, the only hot corino source investigated in detail until now (Caux et al. 2011; Jaber et al. 2014; Jørgensen et al. 2016; Jaber Al-Edhari et al. 2017). In order to avoid possible bias in the analysis, we take into account only the molecular transitions detected at an angular scale comparable to that of the ASAI survey (10–30 arcsec) and in the same spectral range.

The chemical richness can be first described by the number of detected main isotopologues in the ASAI sources, as shown in Table 5. It is typically 40, ranging from 35 (SVS13A) to 51 (B1b). This number varies little between sources, independently of their evolutionary stage and luminosity. Overall, there is no marked difference between the relative importance of the different chemical families.

The ratio r of O-bearing/hydrocarbon *species* allows us to discriminate between the hot corino sources ($r \simeq 1.9$–3.8) and the WCCC sources ($r \simeq 1.0$–1.4). The definitions adopted for the O- and C-families are very conservative but offer the advantage of lifting any ambiguity on the value of r and r^* (see below). We observe that the ratio r tends to increase with time, from FHSC ($r = 1.9$) to Class I ($r = 2.3$). Based on this ratio, we could classify L1157-mm as a WCCC source ($r = 1.4$) and B1b and SVS13A as hot corino sources ($r = 1.9$ and 2.3, respectively), in agreement with the inventory of detected complex organic molecules (see Table 2). As can be seen in Table 5 and Fig. 4, the difference between O-rich and hydrocarbon-rich sources appears markedly when considering the ratio r^* of the number of molecular *lines* from O- to C-bearing species. The range of values is $r^* = 0.3$–1.5 for WCCC sources and $r^* = 2.2$–8.6 for hot corino sources.

A trend seems to emerge between the chemical properties of the envelopes and the location of the protostars inside the molecular clouds. The large Submillimetre Common-User Bolometer Array (SCUBA) survey of the Perseus molecular cloud by Hatchell et al. (2005) shows that the three hot corino sources of our sample (B1b,

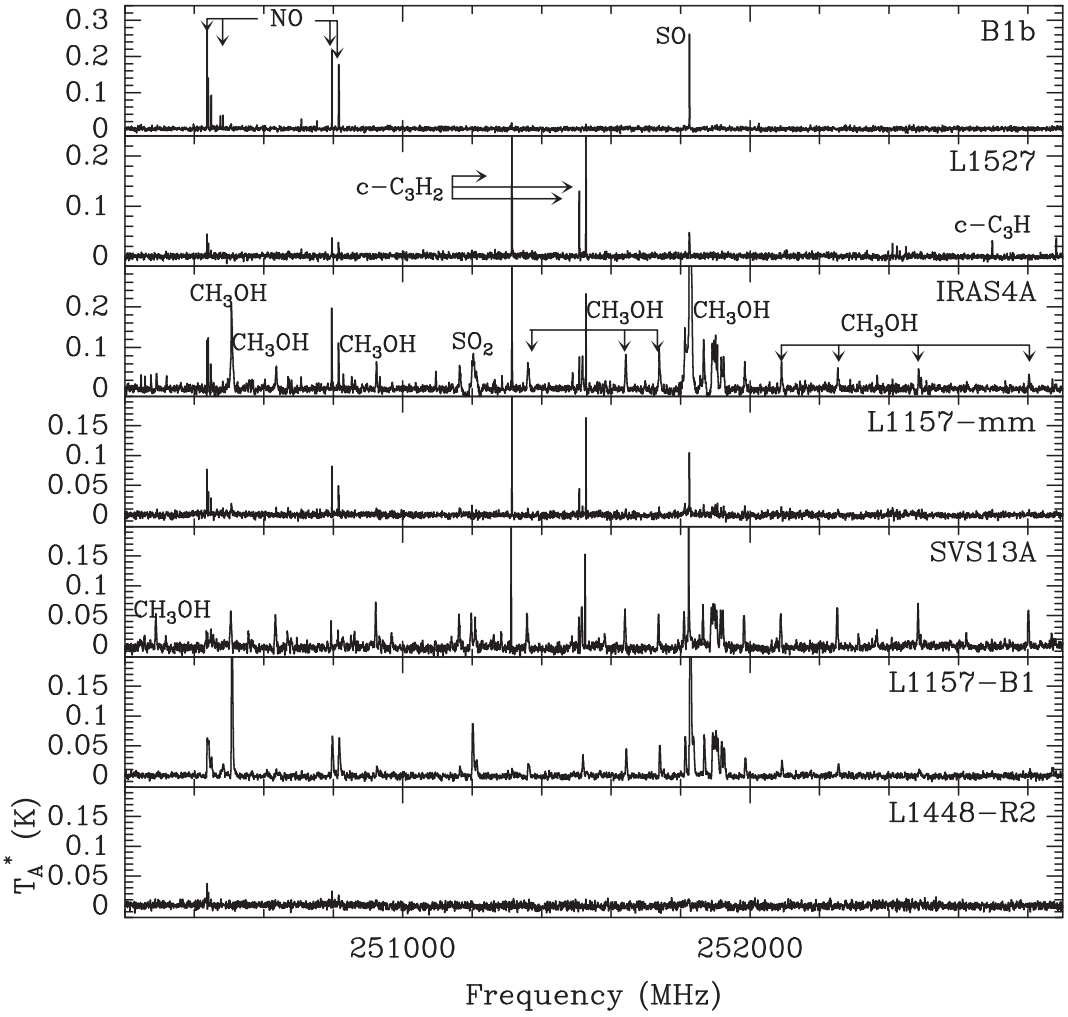

Figure 3. Molecular line emission detected with ASAI in the spectral bands 250200–252900MHz. The spectral resolution is 700 kHz for all the sources, except L1157-B1 (780 kHz).

IRAS4A, and SVS13A) are located inside dense filamentary clouds (see also Sadavoy et al. 2014). This is unlike L1527, which is located outside the dense filaments of the Taurus molecular cloud (Goldsmith et al. 2008) and L1157-mm, which lies in a small isolated cloud (see e.g. Chiang et al. 2010). This suggests that environmental conditions could play an important role in the origin of the chemical protostellar diversity. Systematic studies on a much larger sample should be carried out in order to confirm this trend.

Two ASAI sources display a low content in carbon-bearing species: SVS13A and L1157-B1. It is difficult to conclude if this is a consequence of specific chemical activity associated with outflows, or simply a time evolution effect, or both.

Since many sources are associated with outflow shock regions inside the telescope beam, it may seem not so surprising that many lines and species are detected in common towards protostars and pure outflow shock regions. However, the two protostellar shocks studied here display unexpected results: L1157-B1 (in a WCCC protostellar region) has a signature typical of hot corino regions ($r = 3.8$), a fact confirmed by the large number of detected COMs in the shock (Lefloch et al. 2017), whereas L1448-R2, associated with a hot corino region, has a signature typical of WCCC ($r = 1.3$). Detailed analysis of the chemical conditions in L1448-R2 is currently going on to understand why so many C-chains are still present in the shock.

The number of detected S-bearing species is rather constant. CH_3SH is the only S-bearing COM in the ASAI sample. D-isotopologues are detected at all stages of evolution. The number of deuterated species is found quite high in the pre-stellar and Class 0 phase, before dropping in the advanced Class I phase (Bianchi et al. 2017). Many deuterated species are in both shocks, which reveal the presence of fossil deuteration in the outflowing gas (see Codella et al. 2012).

Overall, we detect from ≈200 to 400 molecular lines per source in the 3 mm band. The number of detected molecular lines increases with source luminosity in the early protostellar stage, and decreases with evolutionary stage, from Class 0 to Class I. We do not observe any marked difference in terms of spectral line density between pre-stellar and protostellar objects, with $\sigma \simeq 6-12$ lines GHz^{-1} (Table 5). Unexpectedly, the spectral line density measured in protostellar shocks and pre-stellar cores is comparable to that measured towards protostars: the lowest spectral line density is measured towards the lower luminosity protostars and/or more evolved protostars.

Table 2. 3 mm band observations: census of detected molecular species classified per elemental family: oxygen, nitrogen, carbon, and sulfur. In a few cases marked with a †, species were detected through the emission of their rare isotopologues (D, ^{13}C). In a few cases, species missed by ASAI in the 3 mm band were known to be present thanks to their signature in the 2 and 1.3 mm bands, like SO^+ or H_2CO. These few species are marked with an *. O- and N-bearing COMs are marked in boldface. For each molecular species, we indicate the associated TAG, according to the data base used for identification (CDMS or JPL). In the last column, we have reported the molecular content of the IRAS 16293−2422 envelope based on the TIMASS survey (Caux et al. 2011).

		L1544	B1b	L1527	IRAS4A	L1157-mm	SVS13A	L1157-B1	L1448-R2	IRAS 16293	TAG
O-	CO	Y	Y	Y	Y	Y	Y	Y	Y	Y	28503
	HCO	Y	Y	Y	Y	Y	Y	Y	Y	Y	29004
	HCO^+	Y	Y	Y	Y	Y	Y	Y	Y	Y	29507
	$HOCO^+$	Y	Y	Y	Y	Y	–	Y	Y	–	45010
	H_2O	[a]	–	[b]	†	–	†	†	[c]	†	19004
	CCO	–	Y	–	–	–	–	–	–	–	40006
	CCCO	Y	Y	Y	–	–	–	–	–	–	52501
	CH_3OH	Y	Y	Y	Y	Y	Y	Y	Y	Y	32003
	H_2CO	†	†	†	Y	*	Y	Y	*	Y	30501
	H_2COH^+	Y	[d]	–	Y	–	–	Y	–	–	31504
	H_2CCO	Y	Y	Y	Y	Y	–	Y	Y	Y	42501
	HCOOH	Y	Y	–	Y	Y	–	Y	Y	Y	46005
	C_2H_5OH	–	–	–	Y	–	–	Y	–	–	46004
	HCCCHO	Y	Y	Y	Y	–	–	–	–	–	54007
	CH_3CHO	Y	Y	Y	Y	Y	Y	Y	Y	Y	44003
	$HCOOCH_3$	Y	Y	–	Y	–	Y	Y	–	Y	60003
	CH_3OCH_3	Y	Y	–	Y	–	Y	Y	–	Y	46514
		–	–	–	Y	–	–	Y	–	–	60501
	$HCOCH_2OH$										
N-	CN	†	Y	*	Y	*	Y	Y	Y	Y	26001
	HCN	Y	Y	Y	Y	Y	Y	Y	Y	Y	27501
	HNC	Y	Y	Y	Y	Y	Y	Y	Y	Y	27002
	$HCNH^+$	Y	*	*	Y	*	–	–	*	–	28504
	HNO	Y	Y	Y	–	–	–	Y	–	Y	31005
	NH_3†	Y	Y	Y	Y	Y	Y	Y	Y	Y	18004
	N_2H^+	Y	Y	Y	Y	Y	Y	Y	Y	Y	29506
	HC_3N	Y	Y	Y	Y	Y	Y	Y	Y	Y	51501
	HCCNC	Y	Y	Y	Y	–	Y	–	Y	Y	51004
	HNCCC	Y	–	Y	–	–	–	–	–	–	–
	HNCO	Y	Y	Y	Y	Y	Y	Y	Y	Y	43002
	HCNO	Y	Y	Y	Y	Y	–	Y	–	–	43509
	HOCN	Y	Y	Y	Y	Y	–	–	–	–	43510
	HSCN	–	Y	Y	Y	–	–	–	–	–	59505
	HC_3NH^+	Y	Y	–	–	–	–	–	–	–	52503
	HC_5N	Y	–	Y	–	Y	Y	Y	Y	Y	75503
	CH_2CN	Y	Y	Y	–	–	Y	Y	–	–	40505
	CH_3CN	Y	Y	Y	Y	Y	Y	Y	Y	Y	41505
	C_2H_3CN	Y	–	Y	–	–	–	Y	–	–	53515
	NH_2CHO	–	–	–	Y	–	Y	Y	Y	Y	45512
	CCCN	Y	Y	Y	–	–	–	Y	Y	–	50511
C-	CCH	Y	Y	Y	Y	Y	Y	Y	Y	Y	25501
	c-C_3H	Y	Y	Y	Y	Y	–	–	Y	Y	37003
	l-C_3H	Y	Y	Y	Y	Y	–	–	Y	Y	37501
	c-C_3H_2	Y	Y	Y	Y	Y	Y	Y	Y	Y	38002
	l-C_3H_2	Y	Y	Y	–	Y	–	–	–	–	38501
	l-C_4H_2	Y	Y	Y	–	Y	–	–	Y	–	50503
	C_4H	Y	Y	Y	Y	Y	Y	Y	Y	Y	49503
	C_5H	–	–	Y	–	–	–	–	–	–	61003
	C_6H	–	–	Y	–	–	–	–	–	–	73001
	CH_3CCH	Y	Y	Y	Y	Y	Y	Y	Y	Y	40001
S-	CS	Y	Y	Y	Y	Y	Y	Y	Y	Y	44501
	NS	Y	*	–	Y	Y	–	Y	Y	Y	46515
	SO	Y	Y	Y	Y	Y	Y	Y	Y	Y	48501
	SO_2	Y	Y	Y	Y	Y	Y	Y	Y	Y	64502
	OCS	Y	Y	Y	Y	Y	Y	Y	Y	Y	60503
	CCS	Y	Y	Y	Y	Y	Y	Y	Y	Y	56007
	CCCS	Y	Y	Y	Y	Y	Y	–	Y	Y	68503
	HCS^+	Y	Y	Y	Y	Y	Y	Y	Y	Y	45506

Table 2 – *continued*

	L1544	B1b	L1527	IRAS4A	L1157-mm	SVS13A	L1157-B1	L1448-R2	IRAS 16293	TAG
H_2CS	Y	Y	Y	Y	Y	Y	Y	Y	Y	46509
SO^+	–	Y	–	*	*	*	Y	–	–	48010
CH_3SH	–	Y	–	Y	–	–	Y	–	Y	48510

[a]Caselli et al. (2012); [b]Karska et al. (2013); [c]Nisini et al. (2013); [d]Fuente et al. (2016).

Table 3. 3 mm band observations: census of silicon- and phosphorus-bearing molecular species detected. We have indicated the main isotopologues. For each molecular species, we indicate the associated TAG, according to the data base used for identification (CDMS or JPL).

	Source	L1544	B1b	L1527	IRAS4A	L1157-mm	SVS13A	L1157-B1	L1448-R2	IRAS 16293	TAG
Si-	SiO	–	Y	–	Y	Y	Y	Y	Y	Y	44505
	SiS	–	–	–	–	–	–	Y	–	Y	60506
P-	PN	–	Y	–	Y	–	–	Y	–	Y	45511
	PO	–	–	–	–	–	–	Y	–	–	47507

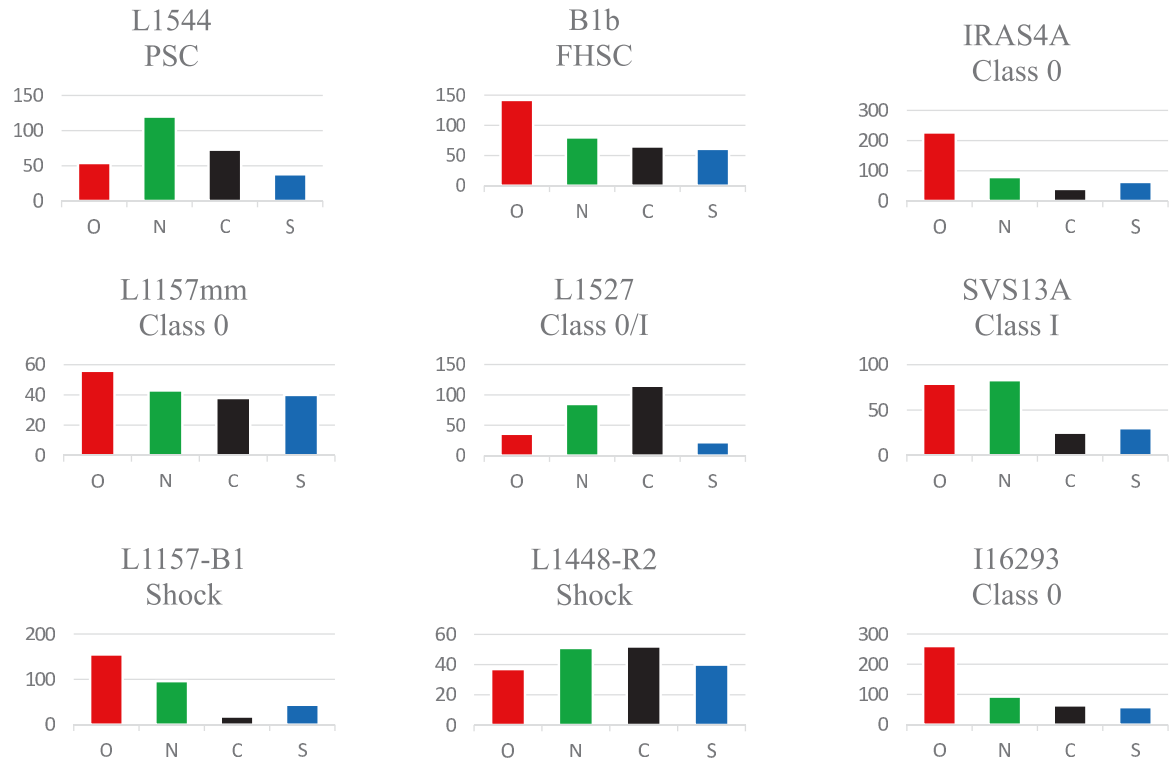

Figure 4. Distribution of the composition of ASAI sources in chemical families, based on the number of molecular lines in the 3 mm band: oxygen, nitrogen, carbon, and sulfur. The early pre-stellar core TMC1 (observed only at 2 mm) was left aside. We show the composition of the Class 0 source IRAS 16293−2422 for the sake of comparison (Caux et al. 2011). Comparison of the C- and O-rich line number permits identification of the WCCC ($O/C \leq 1.5$) and hot corino ($O/C \gg 1.5$) families.

Interestingly enough, the number of main isotopologues detected towards the prototypical hot corino source IRAS 16293−2422 (Caux et al. 2011) and the high-mass star-forming region Orion KL (Tercero et al. 2010) is rather similar to those of the ASAI sources: 41 and 43, respectively. A difference appears when considering the number of lines in the ASAI sources: the number of detected lines in the 3 mm band is typically 200–400, hence fully comparable to that obtained in Class 0 solar-type protostar IRAS 16293−2422, but it is typically a factor of 10 times less than what is found towards Orion KL (Tercero et al. 2010). A similar behaviour was observed in the submillimetre to far-infrared domain by *Herschel* (Ceccarelli et al. 2010), supporting the idea that this result is rather general and frequency independent. Comparing the chemical composition of hot corino sources, only little variations are observed among B1b, IRAS4A, IRAS 16293−2422, and SVS13A (Fig.4). The main difference seems to arise from the content in N-bearing species, relatively more important in Class I SVS13A.

Our main conclusion is that chemical richness is already widely present in the initial phases of solar-type star formation, and it is not less than towards high-mass star-forming regions. Pre-stellar

cores present a high degree of molecular diversity, comparable to that of protostars. The number of detected molecular lines does not appear to depend much on the evolutionary stage of the source. The large difference in spectral line density appears as a consequence of the excitation conditions and not major differences in the chemical richness. Of course, there are strong differences in the molecular abundances even if the species are detected in all sources. In this context, the long studied solar-type protostar IRAS 16293−2422 does not appear to be a unique object, but rather a typical object of the hot corino Class 0, when compared with the other sources of the ASAI sample.

4.2 Unidentified lines

For each source, a few lines detected at the 5σ level remain unidentified (U) in the 3 mm band. Other U lines are present in the spectral surveys, though at a lower level of detection (3σ and 4σ), which cast some doubts on their statistical significance. In order to provide a list of useful and reliable U lines for future spectroscopic work, we have chosen the 5σ level as detection criterion.

The number of U lines per source is low (Table 4) and represents 1–2 per cent of the number of detected lines (per source). In Table5, we report the frequency and observational parameters of these U lines. The reported frequency was chosen so that the emission peak velocity coincides with the $v_{\rm lsr}$ of the source. The uncertainty on the frequency is typically 0.3 MHz ($\approx$1 km s^{-1}) for regions associated with velocity gradients, such as L1157-B1 or L1448-R2. Some U lines were known from previous works. We have indicated the original reference whenever the case in Table 4. There is little match between the list of U lines identified in the different sources, but this is mainly a consequence of our selection criterion, as we report here only the lines detected above the 5σ level.

In the case of L1157-B1, we detected only one line without any proper identification from the JPL and CDMS public line catalogues. We do not confirm any of the U lines reported by Yamaguchi et al. (2012) in their NRO 45 m survey of the shock. The higher sensitivity of the IRAM 30 m data, typically a factor of 5, gives us confidence in our conclusion.

The low number of U lines present in the 3 mm spectral band indicates that they are probably due to 'small' molecules (molecules with a low number of atoms), as opposed to COMs. The content of the 2 and 1.3 mm bands remains to be analysed. Making use of the additional information contained in the higher frequency bands, we hope that collaborations with experts in molecular spectroscopy will allow us to identify the carriers of these U lines.

This is illustrated by our recent identification of the U line at 100198.5MHz, which is detected in several sources: the shock region L1157-B1, the envelope of the driving protostar L1157-mm, the Class 0 protostar IRAS4A, and the FHSC B1b. This line is detected in other sources, like in L1544, with a lower SNR. Using complementary frequency laboratory measurements, we could assign this line to the rotational transition J = 2−1 of NS^+, and we could identify the additional transitions J = 3−2 and J = 5−4 in the ASAI spectra (Cernicharo et al. 2018).

5 CHEMICAL EVOLUTION ALONG STAR FORMATION

From our results it emerges a relatively simple picture of the chemical evolution during the star formation process, which will be depicted here.

5.1 Pre-stellar cores

Observations of the molecular composition of pre-stellar cores, the simplest sites where solar-type stars form, have revealed a very systematic pattern of chemical differentiation (Bergin & Tafalla 2007; Ceccarelli et al. 2007; Caselli & Ceccarelli 2012). During the cold and dense pre-collapse phase, molecules freeze-out on to the grain surfaces, forming ices. Subsequent hydrogenation of atoms and CO on the grain surface leads to the formation of more complex organic molecules, like formaldehyde (H_2CO) and methanol (CH_3OH), in addition to other hydrogenated species (Watanabe, Shiraki & Kouchi 2003; Watanabe et al. 2007; Fuchs et al. 2009; Pirim & Krim 2010; Taquet, Ceccarelli & Kahane 2012; Rimola et al. 2014).

The first results from ASAI reveal that even the dense cores, which are usually assumed to be particularly simple, are much more complex and chemically rich than previously thought. The spectrum of the pre-stellar cores is particularly rich in the 3 mm band, and it is dominated by carbon-containing molecules. From the L1544 spectral scan we have been able to obtain a full census of the oxygen-bearing COMs in this source. We have detected tricarbon monoxide (C_3O), methanol (CH_3OH), acetaldehyde (CH_3CHO), formic acid (HCOOH), ketene (H_2CCO), and propyne (CH_3CCH) with abundances varying from 5×10^{-11} to 6×10^{-9} (Vastel et al. 2014); it was found that a non-thermal desorption mechanism is possibly responsible for the observed emission of methanol and COMs from the same external layer. Subsequent targeted observations have confirmed the presence of a variety of COMs, including methyl formate ($HCOOCH_3$) and dimethyl ether CH_3OCH_3 (Jiménez-Serra et al. 2016). Methanol maps of L1544 by Bizzocchi et al. (2014) confirmed that the emission mainly arises from the outer parts of the core, where CO just started to freeze-out on to dust grains. Similar results on the presence of COMs in dark clouds and pre-stellar cores were obtained by other groups approximately at the same time (Öberg et al. 2010; Bacmann et al. 2012; Cernicharo et al. 2012). Based on the Wideband High-resolution IRAM 30-m Surveys at two Positions with Emir Receivers (WHISPER) survey of the Horsehead Nebula and a nearby dark core, Guzman et al. (2014) reached the same conclusion about the origin of CH_3OH emission: it is present mainly in the envelope. The authors conclude that a pure gas phase model can account for the observed abundance of H_2CO.

The ASAI detection of the cyanomethyl radical (CH_2CN) for the first time in a prototypical pre-stellar core (L1544) was reported by Vastel et al. (2015b). The authors were able to identify the hyperfine transitions of the ortho and para forms and computed all transition frequencies and line intensities for all transitions including satellite hyperfine components at the frequencies observed by ASAI. That paper also reported the first detection of the fine and hyperfine structure of the ortho and para forms of the cyanomethyl radical at 101 GHz, resolved in this cold dense core.

Several molecular ions have been identified. Lines from the protonated carbon dioxide ion, $HOCO^+$, were analysed under non-local thermodynamic equilibrium (LTE) assumptions showing that the $HOCO^+$ emission originates in the same external layer where non-thermal desorption of the other species mentioned above has been observed. Its abundance relative to H_2 is found to be $(5 \pm 2) \times 10^{-11}$, and pure gas phase models of the chemistry involved in the formation and destruction of $HOCO^+$ provide a gaseous CO_2 abundance of 2×10^{-7} (with respect to H_2) with an upper limit of 2×10^{-6} (Vastel et al. 2016). Nitrogen ions such as $HCNH^+$ and HC_3NH^+ have also been detected for the first time in a pre-stellar core (Quénard

Table 4. Frequency and observational parameters of U lines in the ASAI source sample. The observational parameters [flux, linewidth full width at half-maximum (FWHM), and peak flux T_A^*] were obtained from a simple Gauss fit to the line profile. The uncertainties are given in brackets. Velocity-integrated fluxes and line intensities are expressed in units of antenna temperature corrected for atmospheric attenuation. Previously detected lines are commented.

Source	Rest frequency (MHz)	Flux (mK km s^{-1})	FWHM (km s^{-1})	T_A^* (mK)	Comment
L1544	83289.27	7(1)	0.32(0.05)	20.1(2.8)	
	86001.00	6(1)	0.49(0.09)	11.7(2.3)	
	86978.65	8(1)	0.63(0.11)	13.6(2.6)	Previously seen by Jones et al. (2007)
B1b	81571.8	59(8)	1.28(0.17)	43.2(5.6)	
	82395.0	96(9)	1.67(0.17)	53.9(5.3)	
	91344.0	32(5)	3.18(0.60)	9.6(1.7)	
	100198.5	56(3)	1.27(0.09)	42.1(2.2)	
L1527	91425.8	21(4)	1.1(0.2)	19.5(3.5)	
	98832.9	26(5)	1.7(0.4)	13.5(3.5)	
IRAS4A	85294.8	20(4)	1.2(0.3)	16.0(2.9)	
	90669.8	18(3)	1.6(0.3)	11.0(1.8)	Previously seen by Ziurys (1987)
	91359.0	38(4)	1.6(0.1)	22.2(2.6)	
	100198.5	25(2)	1.2(0.1)	19.8(2.4)	
	112563.3	40(8)	1.8(0.4)	21.1(5.7)	
L1157-mm	94500.0	18(4)	1.5(0.4)	11.0(3.0)	Previously seen by Snyder et al. (2002)
	100198.5	17(3)	1.4(0.3)	11.3(2.4)	
	110575.9	66(14)	1.6(0.4)	40.0(9.8)	Previously seen by Combes et al. (1996)
SVS13A	93187.16	31(4)	1.4(0.2)	20.7(1.8)	
	95849.59	17(3)	1.6(0.3)	9.9(2.1)	
L1157-B1	100198.5	46(6)	5.3(0.8)	8.2(1.6)	
L1448-R2	89974.9	59(9)	4.8(0.9)	11(3)	
	92374.0	27(6)	1.3(0.3)	20(4)	

et al. 2017). The high spectral resolution of the observations allows to resolve the hyperfine structure of $HCNH^+$. A radiative transfer modelling of these ions leads to abundances of 3×10^{-10} for $HCNH^+$ and $(1.5-3)\times 10^{-12}$ for HC_3NH^+, with respect to H_2. The study of some nitrogen species linked to their production (HCN, HNC, and HC_3N) coupled with a gas-grain chemical modelling shows that the emission of these ions originates in the external layer where non-thermal desorption of other species was previously observed.

5.2 Protostars

The spectrum of Barnard 1, a protostellar object intermediate between pre-stellar cores and Class 0 sources, is characterized by many lines of deuterated species, complex molecules, and sulfur-bearing molecules. Fuente et al. (2016) provided a very complete inventory of neutral and ionic C-, N-, and S-bearing species with, including the detections of $HOCO^+$ and $HCNH^+$, a tentative detection of HC_3NH^+, and up to our knowledge, the first secure detections of the deuterated ions DCS^+ and $DOCO^+$. The authors also determined the value of the cosmic ray ionization rate and the depletion factors. The observational data were well fitted with ζ_{H_2} between 3×10^{-17} and 10^{-16} s^{-1}. Elemental depletions were estimated to be ∼10 for C and O, ∼1 for N, and ∼25 for S. B1b presents similar depletions of C and O than those measured in pre-stellar cores. The depletion of sulfur was found to be higher than that of C and O but not as extreme as in cold cores. In fact, it is similar to the values found in some bipolar outflows, hot cores, and photon-dominated regions, which could be the consequence of the initial conditions (important outflows and enhanced ultraviolet fields in the surroundings) and a rapid collapse (∼0.1 Myr) that permits to maintain most S- and N-bearing species in gas phase to great optical depths.

The line emission of c-C_3H_2 and its ^{13}C isotopic species were found particularly interesting in the WCCC source L1527, so we conducted a study that confirms the dilution of the ^{13}C species in carbon-chain molecules and their related molecules (Yoshida et al. 2015). The rare isotopologues are thought to originate from C^+, which is diluted in the ^{13}gas phase due to the isotope exchange reaction: $^{13}C^+ + {}^{12}CO \rightarrow {}^{12}C^+ + {}^{13}CO$. This exchange reaction is exothermic ($\Delta E = 35$ K) so that the $^{12}C^+/^{13}C^+$ ratio tends to be higher in cold clouds and the ^{13}C species of various molecules produced from $^{13}C^+$ become less abundant. Moreover, the abundances of the two ^{13}C isotopic species are different from each other. The ratio of c-$^{13}CCCH_2$ species relative to c-$CC^{13}CH_2$ is determined to be 0.20 ± 0.05. If ^{13}C were randomly substituted for the three carbon atoms, this ratio would be 0.5. Hence, the observed ratio indicates that c-$^{13}CCCH_2$ is favoured in dense cores.

The high-sensitivity spectrum obtained towards the Class 0 source L1157-mm looks very similar to that of L1527, and does not display the COM-rich spectrum of objects like IRAS4A (see Figs 1–3). This leads to classify L1157-mm as another member of the WCCC class. The long carbon chains C_5H and C_6H were not detected in the protostellar envelope of L1157-mm. It would be useful to carry out complementary observations in the low frequency range, in which their rotational transitions are more easily detected (see e.g. Sakai et al. 2008), in order to confirm their presence or not. The L1157-mm spectrum also reveals blue and red detached components about 45 km s^{-1} away from the ambient cloud in the profiles of the SiO(5-4) and SiO(6-5) lines (Tafalla et al. 2015). These extremely high-velocity (EHV) components are similar to those found in the L1448 and IRAS 04166+2706 outflows and probably arise

Table 5. 3 mm band observations: number of molecular species (main isotopologue), molecular transitions, and spectral line density σ (in lines GHz^{-1}) for each source of the ASAI sample. We have included IRAS 16293−2422 for comparison. O-COMs: CH_3OH, HCCCHO, $HCOOCH_3$, CH_3OCH_3, and $HCOCH_2OH$; N-COMs: HC_5N, CH_3CN, C_2H_3CN, and NH_2CHO.

Source Type	L1544 PSC	B1b FHSC	L1527 Class 0/I	IRAS4A Class 0	L1157-mm Class 0	SVS13A Class I	L1157-B1 Shock	L1448-R2 Shock	IRAS 16293 Class 0
O-	14	15	10	16	10	9	15	9	11
N-	19	16	19	14	12	12	15	13	12
C-	8	8	10	6	7	4	4	7	6
S-	9	10	8	10	11	9	9	9	9
Si-	0	1	0	1	1	1	2	2	2
P-	0	1	0	1	0	0	2	0	1
Total species	50	51	47	48	41	35	47	40	41
D-	11	18	11	11	7	3	3	8	13
r (O-/C-lines)	1.8	1.9	1.0	2.7	1.4	2.3	3.8	1.3	1.8
O-lines	54	142	36	227	56	79	155	37	260
N-lines	124	80	85	79	43	83	96	51	93
C-lines	73	65	115	40	38	25	18	52	64
S-lines	38	61	22	63	40	30	44	40	58
Si-lines	0	1	0	3	1	1	6	4	3
P-lines	0	1	0	1	0	0	5	0	1
Total lines	289	350	258	413	178	218	324	184	479
D-lines	47	62	46	75	31	15	5	30	79
r^* (O-/C-lines)	0.7	2.2	0.3	5.7	1.5	3.2	8.6	0.7	4.1
O-COMs lines	35	109	14	197	36	63	139	27	244
N-COMs lines	32	7	16	23	7	21	46	10	38
U lines	3	4	2	5	3	2	1	2	–
U lines/total lines (per cent)	1.0	1.2	0.8	1.2	1.7	0.9	0.3	1.0	–
σ (lines GHz^{-1})	8.9	11.0	8.0	11.8	5.3	6.1	9.1	5.8	13.3

from a molecular jet driven by L1157-mm that excites L1157-B1 and the other chemically active spots of the L1157 outflow. This jet was recently mapped with NOEMA by Podio et al. (2016).

A very interesting result from ASAI is that the phase of hot corino can persist until the phase of Class I, as illustrated by the observations of SVS13A (Codella et al. 2016). In the spectrum of SVS13A, we clearly detected six broad (FWHM $\sim$ 4–5 km s^{-1}) emission lines of HDO with upper level energies up to $E_u = 837$ K (Codella et al. 2016). A non-LTE large velocity gradient (LVG) analysis implies the presence of very hot (150–260 K) and dense ($>3 \times 10^7$ cm^{-3}) gas inside a small radius ($\sim$25 au) around the star, which is a clear indication, for the first time, of the occurrence of a hot corino around a Class I protostar. Although the effects of shocks and/or winds at such small scales cannot be excluded, this could imply that the observed HDO emission is tracing the water abundance jump expected at temperatures $\sim$220–250 K, when the activation barrier of the gas phase reactions leading to the formation of water can be overcome. We derive X(HDO) $\sim 3 \times 10^{-6}$, and a H_2O deuteration $>1.5 \times 10^{-2}$. The presence of a hot corino was confirmed by Bianchi et al. (2017), who showed evidence for a methanol-enriched small region (radius $\simeq$ 35 au) of hot ($T \sim 80$ K) and dense gas ($n(H_2) \geq 10^8$ cm^{-3}) around the protostar. More importantly, the analysis of the emission of the deuterated isotopologues of H_2CO and CH_3OH showed that the deuteration richness drops in the Class I phase. Recent observations with the Plateau de Bure Interferometer at 0.3 arcsec showed that the hot corino emission actually arises from component VLA4B of the binary (Lefèvre et al. 2017).

5.3 Protoplanetary phase

In the subsequent phases (Class I/II), the envelope dissipates as the matter accretes on to the central object and is dispersed by the outflow/jet, as the surrounding protoplanetary disc becomes detectable. Chemistry is expected to be somewhat similar to that of Class 0 sources, with a corino region where ices sublimate, and to the pre-stellar cores, in the cold and dense regions close to the equatorial plane.

The spectral line density of AB Aur is very low, as expected in a protoplanetary disc. Nevertheless, several lines of CO and its isotopologues, HCO^+, H_2CO, HCN, CN, and CS, were detected (Pacheco-Vásquez et al. 2015). In addition, the detection of the SO 5_4–3_3 and 5_6–4_5 lines confirms the previously tentative detection of Fuente et al. (2010), which makes AB Aur the only protoplanetary disc detected in SO. This detection indicates that this disc is warmer and younger than those associated with T Tauri stars. These ASAI results prompted follow-up studies at very high resolution that revealed the detailed structure of the AB Aur disc (Pacheco-Vásquez et al. 2016).

5.4 Outflow shocks

Simultaneously with matter accretion on to the protostar, fast jets, possibly surrounded by a wider angle wind, are powered by the nascent star and seen to interact with the parental medium through molecular bow shocks, producing a slower moving molecular 'outflow cavity' (Bachiller 1996). Outflow shocks compress and heat the

interstellar material and grain ice mantles are sputtered, resulting in an especially rich chemistry (Bachiller et al. 2001; Codella et al. 2010). The EHV gas-forming 'molecular bullets' are well differentiated from the gas traced by the standard outflow cavity wings and could represent material directly ejected from the protostar or its immediate vicinity (Tafalla & Bachiller 2011). Outflows contribute to dissipate the circumstellar envelope, permitting the radiation of the central object to escape at increasing distances, until the central star and its surrounding protoplanetary disc become optically visible as a (Class II) T Tauri star.

The L1157-B1 hotspot exhibits a particularly rich spectrum with hundreds of lines of many different molecular species (see Table 2), which makes it an ideal laboratory not only for shock but also for astrochemical studies. Most of the lines tentatively detected by the NRO 45 m telescope could be confirmed by ASAI (see table3 in Yamaguchi et al. 2012), in particular the tentative detections of $Si^{18}O$ and SiS. There are two exceptions however: first, Lefloch et al. (2017) assigned the transition CH_3OCHO 7(4,4,1)-6(4,3,1) to the line at 86224.16MHz, instead of $(CH_3)_2O$ at 86223.78MHz; second, Mendoza et al.(2014) assigned the transitions HCNO 4-3 to the line at 91751.32MHz, instead of HSCN 8(0,8)-7(0,7), in agreement with the detection of HCNO 5-4 at 114688.38MHz (Mendoza et al. 2014). Several species are now detected, including complex N-bearing species (C_2H_3CN and CH_2CN), long carbon-chain molecules ($CH_4$and HC_5N), and deuterated molecules like HDCS, NH_2D, or HDO (see also Codella et al. 2012).

Podio et al. (2014) presented a complete census of molecular ions with an abundance greater than $\sim 10^{-10}$, reporting the detection of HCO^+, $H^{13}CO^+$, N_2H^+, HCS^+, and for the first time in a shock, from $HOCO^+$ and SO^+. It was concluded that HCO^+ and N_2H^+ are a fossil record of pre-shock gas in the outflow cavity, whilst $HOCO^+$, SO^+, and HCS^+ are effective shock tracers that can be used to infer the amount of CO_2 and sulfur-bearing species released from dust mantles in the shock. The work on sulfur-bearing ions predicted OCS to be a major carrier of sulfur on dust mantles and modelling of H_2S observations suggest H_2S should not be a major carrier of sulfur on the grains (Holdship et al. 2016).

A multiline analysis of CS and its isotopic variations allowed to study the density structure of the molecular outflow (Gómez-Ruiz et al. 2015). The line profiles can be well fitted by a combination of two exponential laws that are remarkably similar to what previously found using CO by Lefloch et al. (2012). The CS observations show that this molecule is highlighting the dense, $n_{H_2} = 1–5\times 10^5$ cm^{-3}, cavity walls produced by the episodic outflow in L1157. In addition, the highest excitation ($E_u \geq$ 130 K) CS lines provide us with the signature of denser (1–5$\times$ 10^6 cm^{-3}) gas, associated with a molecular reformation zone of a dissociative J-type shock, which is expected to arise where the precessing jet impacting the molecular cavities. The CS fractional abundance increases up to 10^{-7} in all the kinematical components. This value is consistent with what previously found for prototypical protostars and it is in agreement with the prediction of the abundances obtained via chemical modelling.

Podio et al. (2017) reported the detection of SiS for the first time in a low-mass-forming region, in particular the protostellar shock L1157-B1. Complementary observations of the shock obtained with the Plateau de Bure Interferometer show for the first time that SiO and SiS have a different spatial distribution. Although SiO is a well established probe of silicates released from dust grain in shocks (see e.g. Gusdorf et al. 2008), SiS appears as a product of gas phase reactions between species released from dust grains in the shock. There is currently no satisfying formation scenario and more work is needed to understand the chemistry of Si-bearing molecules.

Thanks to the high sensitivity of the ASAI observations and full coverage of the 1.3, 2, and 3 mm wavelength bands, a systematic search by Lefloch et al. (2017) led to the unambiguous detection of several COMs, such as ketene (H_2CCO), dimethyl ether (CH_3OCH_3), and glycolaldehyde ($HCOCH_2OH$) for the first time, and other tentative detections (Arce et al. 2008) were firmly confirmed, such as formic acid (HCOOH) and ethanol (C_2H_5OH). The large number of detected lines from each species ($\sim$10–125) permitted accurate determination of their excitation conditions and molecular abundances. Combining these results with those previously obtained towards other protostellar objects, a good correlation is observed between ethanol, methanol, and glycolaldehyde. The COM richness of the shock region L1157-B1 is fully comparable to that observed in hot corinos, both in terms of molecular abundances and chemical diversity. The potential of shocks to study pre-biotic chemistry is illustrated by the detection of formamide (NH_2CHO) in L1157-B1 by Mendoza et al. (2014). This species is detected in a wide range of Galactic and extragalactic environments. It turns out that the abundance in the L1157-B1 shock region, $\approx 5 \times 10^{-9}$, is among the highest values reported.

5.5 Pre-biotic molecules along protostellar evolution

López-Sepulcre et al. (2015) have conducted some first comparative studies for molecular species of particular interest, such as isocyanic acid (HNCO) and formamide. HNCO was detected in all the ASAI targets, except AB Aur, and NH_2CHO in five of them. Their abundances were derived and analysed them together with those reported in the literature for high-mass sources. For those sources with formamide detection, a tight and almost linear correlation was found between HNCO and NH_2CHO abundances, with their ratio being roughly constant, suggesting that the two species are chemically related. The sources without formamide detection, which are also the coldest and devoid of hot corinos, fall well off the correlation, displaying a much larger amount of HNCO relative to NH_2CHO. These results suggest that HNCO can be formed in the gas phase during the cold stages of star formation. On the contrary NH_2CHO forms preferentially in warm environments. Recent theoretical and observational studies (Barone et al. 2015; Skouteris et al. 2017) suggest that formamide could form efficiently in the gas phase from the reaction between NH_2 and H_2CO. The tight correlation observed between formamide and isocyanic acid remains to be understood.

Formamide is one example of molecules of pre-biotic interest, which ASAI has allowed us to search for in solar-type star-forming regions. Another example is provided by the search for phosphorus-bearing species. Despite a low elemental abundance (3×10^{-7}; Asplund et al. 2009), phosphorus plays an important role in biochemical and metabolic processes in living beings. The signature of PN was detected in three sources of ASAI, two of which are protostars (see Table 3). For the first time, PO was detected in a solar-type protostellar shock region (Lefloch et al. 2016). Phosphorus-bearing species have been detected mainly in high-excitation shock regions until now (see also Ziurys 1987), similarly to silicon-bearing species. Their non-detection towards the pre-stellar core L1544 is therefore not surprising. The lack of detection towards L1527 or SVS13A is consistent with shocks of low excitation in the envelope.

6 CONCLUSION

We have undertaken the Large Program ASAI to characterize and to understand the chemical evolution along solar-type protostellar evolution. To do so, we have used the IRAM 30 m telescope to carry out unbiased millimetre line surveys between 80 and 272 GHz of a sample of 10 template sources, which cover the full formation process of solar-type stars, from pre-stellar cores to protoplanetary discs. At the time of writing this paper, the ASAI data analysis is under way and more results on the different sources and transversal studies will be published in forthcoming papers. Below, we summarize our first conclusions based on the analysis of the 3 mm data.

(i) Molecular complexity is already present at early pre-stellar and protostellar stages. The chemical richness is already comparable to that of massive hot core regions, like Orion KL.

(ii) The number of detected molecular species varies little between sources, independently of their evolutionary stage and their luminosity. The number of detected molecular lines increases with source luminosity in the early protostellar stage, and decreases with evolutionary stage, from Class 0 to Class I. We do not observe any marked difference in terms of spectral line density between pre-stellar and protostellar phase. Unexpectedly, the spectral line density measured in protostellar shocks is fully comparable to that measured towards protostars.

(iii) The ratio of O- to C-bearing species/lines allows to identify very well the hot corino from the WCCC sources. This has permitted identification of a new WCCC (L1157-mm) and hot corino (SVS13A and B1b) sources.

(iv) The hot corino sources of our sample are located inside dense filamentary clouds, whereas the WCCC sources are located outside dense filamentary structures.

(v) The census of deuterated isotopologues shows similar number of detected species in the pre-stellar and early (Class 0) protostellar phase, independently of the chemical protostellar type (hot corino versus WCCC).

(vi) Our analysis provides a first glimpse on the pre-biotic chemistry at work in solar-type star-forming regions. Formamide, P-bearing species and glycolaldehyde are detected species of high interest, which deserve further studies.

(vii) COMs are commonly found at all stages of protostellar evolution, including energetic environments such as shocks.

(viii) A few U lines, whose number amount to 1–2 per cent of the total number of detected lines, remain to be identified in the 3 mm band for each source. Such low numbers of U lines imply that we have obtained a comprehensive census of the COMs present in the sources of the sample.

From this preliminary analysis, a relatively detailed picture of the chemical evolution from pre-stellar cores to evolved Class II protostars can be drawn, while opening new questions, which will be addressed in further studies. It is important to confirm whether the difference of environmental conditions between hot corino and WCCC sources (inside/outside dense filamentary cloud regions) is a general trend. If so, it would provide important constraints on the origin of the chemical diversity observed in protostellar envelopes. As a consequence of the limited angular resolution of the survey (≈20 arcsecin the 3 mm band), several physical components may be contributing the detected emission: shocks, disc, hot corino, and cold envelope. Source multiplicity (like in IRAS4A, B1b, or SVS13A) makes it more difficult to interpret the results on the overall chemical evolution of the sources, especially in the case where the sources are at different evolutionary stages. The question as to whether chemical complexity increases, how much it differs in the close environment of protostars, the chemical processing associated with each physical component has to be addressed with higher angular resolution observations. It is one of the goals of the IRAM/NOEMA Large Program 'Seeds Of Life In Space' (SOLIS;[8] Ceccarelli et al. 2017).

Our results also illustrate the critical need of combining laboratory measurements and astronomical observations, as well as the need for a re-evaluation of the chemical processes at work in the gas phase and the characterization of molecular species neglected until now. We also stress the need for the computation of accurate collisional excitation rate coefficients.

In many cases, collisional rates with H_2 are simply not available. As an alternative, collisional rates with He (when available) or more simple hypothesis like LTE are used in order to determine molecular column densities, which therefore suffer some ambiguities in their determination. We hope that the wealth of molecular species commonly observed in the ASAI data base will encourage experts in collisional rate computation to pursue and increase their efforts in the domain.

ACKNOWLEDGEMENTS

We thank an anonymous referee for useful comments and suggestions. We thank Dr A. Faure for discussions on nitrogen isotopologues. This paper is based on observations carried out as part of the Large Program ASAI (project number 012-12) with the IRAM 30 m telescope. IRAM is supported by INSU/CNRS (France), MPG (Germany), and IGN (Spain). This work was supported by the Programme National 'Physique et Chimie du Milieu Interstellaire' (PCMI) of CNRS/INSU with INP/INC, cofunded by CNES and CEA. JC and NM thank Spanish MINECO for funding under grants AYA2012-32032, AYA2016-75066-C2-1/2-P, CSD2009-00038 (ASTROMOL) under the Consolider-Ingenio Program, and acknowledge funding support from the European Research Council ERC Grant 610256: NANOCOSMOS. RB and MT acknowledge support from grant AYA2016-79006-P. EM acknowledges support from the Brazilian agency FAPESP, projects 2014/22095−6 and 2015/22254−0.

REFERENCES

André P., Ward-Thompson D., Barsony M., 1993, ApJ, 406, 122
Arce H. G., Santiago-García J., Jørgensen J. K., Tafalla M., Bachiller R., 2008, ApJ, 681, L21
Asplund M., Grevesse N., Sauval J., Scott P., 2009, ARA&A, 47, 481
Bachiller R., 1996, ARA&A, 34, 111
Bachiller R., Cernicharo J., 1984, A&A, 140, 414
Bachiller R., Cernicharo J., 1986, A&A, 168, 262
Bachiller R., Guilloteau S., Gueth F., Tafalla M., Dutrey A., Codella C., Castets A., 1998, A&A, 339, L49
Bachiller R., Martin-Pintado J., Fuente A., 1993, ApJ, 417, L45
Bachiller R., Martin-Pintado J., Tafalla M., Cernicharo J., Lazareff B., 1990a, A&A, 231, 174
Bachiller R., Menten K. M., del Rio Alvarez S., 1990b, A&A, 236, 461
Bachiller R., Pérez Gutiérrez M., 1997, ApJ, 487, L93
Bachiller R., Pérez Gutiérrez M., Kumar M. S. N., Tafalla M., 2001, A&A, 372, 899
Bacmann A., Taquet V., Faure A., Kahane C., Ceccarelli C., 2012, A&A, 541, L12
Barone V., Latouche C., Skouteris D., Vazart F., Balucani N., Ceccarelli C., Lefloch B., 2015, MNRAS, 453, L31
Bergin E. A., Tafalla M., 2007, ARA&A, 45, 339

[8] http://ipag.osug.fr/solis

Bianchi E. et al., 2017, MNRAS, 467, 3011
Bizzocchi L., Caselli P., Spezzano S., Leonardo E., 2014, A&A, 569, A27
Blake G. A., Sandell G., van Dishoeck E. F., Groesbeck T. D., Mundy L. G., Aspin C., 1995, ApJ, 441, 689
Blake G. A., van Dishoeck E. F., Jansen D. J., Groesbeck T. D., Mundy L. G., 1994, ApJ, 428, 680
Bockelée-Morvan D. et al., 2000, A&A, 353, 1101
Bottinelli S., Ceccarelli C., Williams J. P., Lefloch B., 2007, A&A, 463, 601
Bottinelli S. et al., 2004a, ApJ, 615, 354
Burkhardt A. M. et al., 2016, ApJ, 827, 21
Busquet G. et al., 2014, A&A, 561, A120
Caselli P., Ceccarelli C., 2012, A&AR, 20, 56
Caselli P., Walmsley C. M., Tafalla M., Dore L., Myers P. C., 1999, ApJ, 523, L165
Caselli P. et al., 2012, ApJ, 759, L37
Caux E. et al., 2011, A&A, 532, A23
Cazaux S., Tielens A. G. G. M., Ceccarelli C., Castets A., Wakelam V., Caux E., Parise B., Teyssier D., 2003, ApJ, 593, L51
Ceccarelli C., Caselli P., Bockelée-Morvan D., Mousis O., Pizzarello S., Robert F., Semenov D., 2014, in Beuther H., Klessen R. S., Dullemond C. P., Henning T., eds, Protostars and Planets VI. Univ. Arizona Press, Tucson, AZ, p. 859
Ceccarelli C., Caselli P., Herbst E., Tielens A. G. G. M., Caux E., 2007, in Reipurth B., Jewitt D., Keil K., eds, Protostars and Planets V. Univ. Arizona Press, Tucson, AZ, p. 47
Ceccarelli C. et al., 2010, A&A, 521, L22
Ceccarelli C. et al., 2017, ApJ, 850, 176
Cernicharo J., Guélin M., 1987, A&A, 176, 299
Cernicharo J., Marcelino N., Roueff E., Gerin M., Jiménez-Escobar A., Muñoz Caro G. M., 2012, ApJ, 759, L43
Cernicharo J. et al., 2013, ApJ, 771, L10
Cernicharo J. et al., 2018, ApJ, 853, L22
Chen X., Launhardt R., Henning T., 2009, ApJ, 691, 1729
Chiang H. F., Looney L. W., Tobin J. J., Hartmann L., 2010, ApJ, 709, 470
Choi M., 2001, ApJ, 553, 219
Choi M., 2005, ApJ, 630, 976
Codella C., Fontani F., Ceccarelli C., Podio L., Viti S., Bachiller R., Benedettini M., Lefloch B., 2015, MNRAS, 449, L11
Codella C. et al., 2010, A&A, 518, L112
Codella C. et al., 2012, ApJ, 757, L9
Codella C. et al., 2016, A&A, 586, L3
Combes F., Q-Rieu N., Wlodarczak G., 1996, A&A , 308, 618
Daniel F. et al., 2013, A&A, 560, A3
De Simone M. et al., 2017, A&A, 599, A121
Dutrey A., Guilloteau S., Bachiller R., 1997, A&A, 325, 758
Fuchs G. W., Cuppen H. M., Ioppolo S., Romanzin C., Bisschop S. E., Andersson S., van Dishoeck E. F., Linnartz H., 2009, A&A, 505, 629
Fuente A., Cernicharo J., Agúndez M., Berné O., Goicoechea J. R., Alonso-Albi T., Marcelino N., 2010, A&A, 524, A19
Fuente A. et al., 2016, A&A, 593, A94
Fuente A. et al., 2017, A&A, 606, L3
Gerin M., Pety J., Fuente A., Cernicharo J., Commerçon B., Marcelino N., 2015, A&A, 577, L2
Goldsmith P. F., Heyer M., Narayanan G., Snell R., Li D., Brunt C., 2008, ApJ, 680, 428
Gueth F., Bachiller R., Tafalla M., 2003, A&A, 401, L5
Gueth F., Guilloteau S., Bachiller R., 1996, A&A, 307, 891
Guilloteau S., Di Folco E., Dutrey A., Simon M., Grosso N., Piétu V., 2013, A&A, 549, A92
Gusdorf A., Pineau Des Forêts G., Cabrit S., Flower D. R., 2008, A&A, 490, 695
Guzman V., et al., 2014, Faraday Discuss, 168, 103
Gómez-Ruiz A. I., Wyrowski F., Gusdorf A., Leurini S., Menten K. M., 2013, A&A, 555, A8
Gómez-Ruiz A. I. et al., 2015, MNRAS, 446, 3346
Hatchell J., Richer J. S., Fuller G. A., Qualtrough C. J., Ladd E. F., Chandler C. J., 2005, A&A, 440, 151
Hirano N., Liu C.-F., 2014, ApJ, 789, 50
Hogerheijde M. R., van Dishoeck E. F., Blake G. A., van Langevelde H. J., 1998, ApJ, 502, 315
Holdship J. et al., 2016, MNRAS, 463, 802
Imai M. et al., 2016, ApJ, 830, L37
Jaber A., Ceccarelli C., Kahane C., Caux E., 2014, ApJ, 791, 29
Jaber Al-Edhari A. et al., 2017, A&A, 597, A40
Jiménez-Serra I. et al., 2016, ApJ, 830, L6
Jones P. A., Cunningham M. R., Godfrey P. D., Cragg D. M., 2007, MNRAS, 374, 579
Jørgensen J. K., Favre C., Bisschop S. E., Bourke T. L., van Dishoeck E. F., Schmalzl M., 2012, ApJ, 757, L4
Jørgensen J. K. et al., 2016, A&A, 595, A117
Kahane C., Ceccarelli C., Faure A., Caux E., 2013, ApJ, 763, L38
Karska A. et al., 2013, A&A, 552, A141
Kramer C., Navarrini A., Navarro S., Jones D., Cernicharo J., 2014, IRAM Report on EMIR Ghost Lines
Lefloch B., Castets A., Cernicharo J., Langer W. D., Zylka R., 1998a, A&A, 334, 269
Lefloch B., Castets A., Cernicharo J., Loinard L., 1998b, ApJ, 504, L109
Lefloch B., Ceccarelli C., Codella C., Favre C., Podio L., Vastel C., Viti S., Bachiller R., 2017, MNRAS, 469, L73
Lefloch B. et al., 2010, A&A, 518, L113
Lefloch B. et al., 2012, ApJ, 757, L25
Lefloch B. et al., 2016, MNRAS, 462, 3937
Lefèvre C. et al., 2017, A&A, 604, L1
Lis D. C., Roueff E., Gerin M., Phillips T. G., Coudert L. H., van der Tak F. F. S., Schilke P., 2002, ApJ, 571, L55
Liszt H. S., Ziurys L. M., 2012, ApJ, 747, 55
Looney L. W., Tobin J. J., Kwon W., 2007, ApJ, 670, L131
Lykke J. M. et al., 2017, A&A, 597, A53
López-Sepulcre A. et al., 2015, MNRAS, 449, 2438
López-Sepulcre A. et al., 2017, A&A, 606, A121
Maier D., 2014, IRAM Report on Lab Measurements of EMIR Mixers
Marcelino N., Cernicharo J., Agúnde M., Roueff E., Gerin M., Martín-Pintado J., Mauersberger R., Thum C., 2007, ApJ, 665, L127
Marcelino N., Cernicharo J., Roueff E., Gerin M., Mauersberger R., 2005, ApJ, 620, 308
Marcelino N., Cernicharo J., Tercero B., Roueff E., 2009, ApJ, 690, L27
Mendoza E., Lefloch B., Lopez-Sepulcre A., Codella C., Boechat-Roberty H. M., Bachiller R., 2014, MNRAS, 445, 151
Mumma M. J., Charnley S. B., 2011, ARA&A, 49, 471
Müller H. S. P., Schlöder F., Stutzki J., Winnewisser G., 2005, J. Mol. Structure, 742, 215
Nisini B., Benedettini M., Giannini T., Codella C., Lorenzetti D., di Giorgio A. M., Richer J. S., 2000, A&A, 360, 297
Nisini B. et al., 2013, A&A, 549, A16
Oya Y., Sakai N., Lefloch B., López-Sepulcre A., Watanabe Y., Ceccarelli C., Yamamoto S., 2015, ApJ, 812, 59
Oya Y. et al., 2017, ApJ, 837, 174
Öberg K., Bottinelli S., Jørgensen J., van Dishoeck E., 2010, ApJ, 716, 825
Pacheco-Vásquez S. et al., 2015, A&A, 578, A81
Pacheco-Vásquez S. et al., 2016, A&A, 589, A60
Persson M. V., Jørgensen J. K., van Dishoeck E. F., 2012, A&A, 541, A39
Pezzuto S. et al., 2012, A&A, 547, A54
Pickett H. M., Poynter I. R. L., Cohen E. A., Delitsky M. L., Pearson J. C., Müller H. S. P., 1998, J. Quant. Spectrosc. Radiat. Transf., 60, 883
Pirim C., Krim L., 2010, in International Symposium on Molecular Spectroscopy, 65th Meeting. Ohio State University, Columbus, OH
Pizzarello S., Huang Y., 2005, Geochim. Cosmochim. Acta, 69, 599
Piétu V., Guilloteau S., Dutrey A., 2005, A&A, 443, 945
Podio L., Lefloch B., Ceccarelli C., Codella C., Bachiller R., 2014, A&A, 565, A64
Podio L. et al., 2016, A&A, 593, L4
Podio L. et al., 2017, MNRAS, 470, L16
Pratap P., Dickens J. E., Snell R. L., Miralles M. P., Bergin E. A., Irvine W. M., Schloerb F. P., 1997, ApJ, 486, 862
Quénard D., Vastel C., Hily-Blant P., Ceccarelli C., Lefloch B., Bachiller R., 2017, MNRAS, 470, 3194

Rimola A., Taquet V., Ugliengo P., Balucani N., Ceccarelli C., 2014, A&A, 572, A70
Robitaille T. P., Whitney B. A., Indebetouw R., Wood K., 2007, ApJ , 169, 328
Roueff E., Lis D. C., van der Tak F. F. S., Gerin M., Goldsmith P. F., 2005, A&A, 438, 585
Sadavoy S. I. et al., 2014, ApJ, 787, L18
Sakai N., Sakai T., Hirota T., Yamamoto S., 2008, ApJ, 672, 371
Sakai N., Sakai T., Hirota T., Yamamoto S., 2010, ApJ, 722, 1633
Sakai N., Yamamoto S., 2013 Chem. Rev., 113, 898
Sakai N. et al., 2017, MNRAS, 467, L76
Santangelo G. et al., 2012, A&A, 538, A45
Santangelo G. et al., 2014, A&A, 568, A125
Santangelo G. et al., 2015, A&A, 584, A126
Schlafly E. F. et al., 2014, ApJ, 786, 29
Schreyer K. et al., 2008, A&A, 491, 821
Skouteris D., Vazart F., Ceccarelli C., Balucani N., Puzzarini C., Barone E., 2017, MNRAS , 468, L1
Snyder L. E., Lovas F. J., Mehringer D. M., Miao N. Y., Kuan Y.-J., Hollis J. M., Jewell P. R., 2002, ApJ, 578, 256
Sugimura M. et al., 2011, PASJ, 63, 459
Tafalla M., Bachiller R., 2011, in Cernicharo J., Bachiller R., eds, Proc. IAU Symp. 280, The Molecular Universe. Cambridge Univ. Press, Cambridge, p. 88
Tafalla M., Bachiller R., Lefloch B., Rodríguez-Fernández N., Codella C., López-Sepulcre A., Podio L., 2015, A&A, 573, L2
Takano S. et al., 2011, in Cernicharo J., Bachiller R., eds, Proc. IAU Symp. 280, The Molecular Universe. Cambridge Univ. Press, Cambridge, p. 60
Tang Y.-W., Guilloteau S., Piétu V., Dutrey A., Ohashi N., Ho P. T. P., 2012, A&A, 547, A84
Tang Y.-W. et al., 2017, ApJ, 840, 32
Taquet V., Ceccarelli C., Kahane C., 2012, A&A, 538, A42
Taquet V., Lopez-Sepulcre A., Ceccarelli C., Neri R., Kahane C., Charnley S. B., 2015, ApJ, 804, 81
Tercero B., Cernicharo J., Pardo J. R., Goicoechea J. R., 2010, A&A, 517, A96
Tobin J. J., Hartmann L., Chiang H. F., Wilner D. J., Looney L. W., Loinard L., Calvet N., D'Alessio P., 2013, ApJ, 771, 48
Tobin J. J. et al., 2016, ApJ, 818, 73
van den Ancker M. E., de Winter D., Tjin A., Djie H. R. E., 1998, A&A, 330, 145
Vastel C., Bottinelli S., Caux E., Glorian J.-M., Boiziot M., 2015a, in Martins F., Boissier S., Buat V., Cambrésy L., Petit P., eds, SF2A-2015: Proceedings of the Annual meeting of the French Society of Astronomy and Astrophysics. p. 313.
Vastel C., Caselli P., Ceccarelli C., Phillips T., Wiedner M. C., Peng R., Houde M., Dominik C., 2006, ApJ, 645, 1198
Vastel C., Ceccarelli C., Lefloch B., Bachiller R., 2014, ApJ, 795, L2
Vastel C., Ceccarelli C., Lefloch B., Bachiller R., 2016, A&A, 591, L2
Vastel C., Yamamoto S., Lefloch B., Bachiller R., 2015b, A&A, 582, L3
Watanabe N., Mouri O., Nagaoka A., Chigai T., Kouchi A., Pirronello V., 2007, ApJ, 668, 1101
Watanabe N., Shiraki T., Kouchi A., 2003, ApJ, 588, L121
Watanabe Y., Sakai N., Lindberg J. E., Jørgensen J., Bisschop S. E., Yamamoto S., 2012, ApJ, 745, 126
Yamaguchi T. et al., 2012, PASJ, 64, 105
Yildiz U. A., Kristensen L. E., van Dishoeck E. F., Belloche A., van Kempen T. A., Hogerheijde M. R., Güsten R., van der Marel N., 2012, A&A, 542, A86
Yoshida K., Sakai N., Tokudome T., Watanabe Y., Takano S., Lefloch B., Lopez-Sepulcre A., Yamamoto S., 2015, ApJ, 807, 66
Ziurys L. M., 1987, ApJ, 321, L81

APPENDIX A: EXAMPLES OF CHEMICAL DIFFERENTIATION IN THE ASAI SOURCE SAMPLE

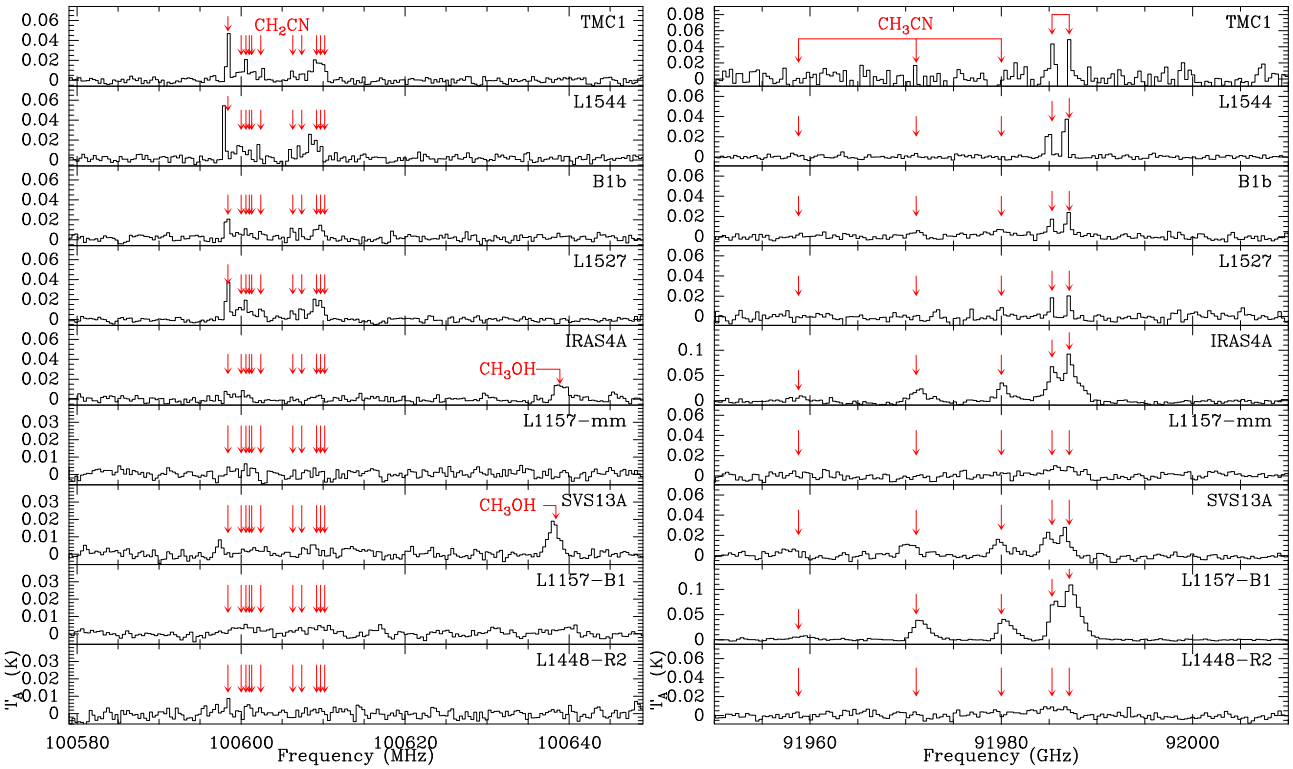

Figure A1. Comparison of CH_2CN (left) and CH_3CN (right) emission line profiles in the 3 mm band. The frequencies of the transitions are marked with arrows.

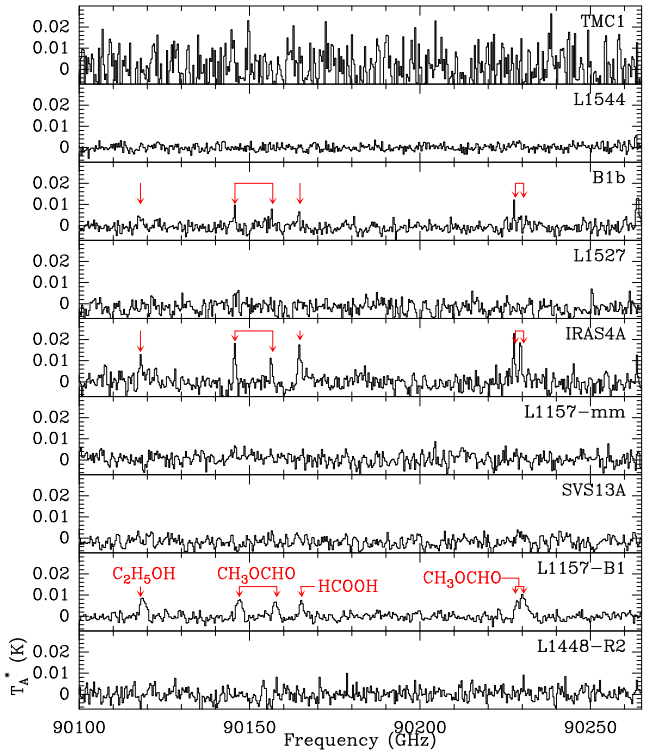

Figure A2. Comparison of COM emission between 90100 and 90255MHz

This paper has been typeset from a TEX/LATEX file prepared by the author..